Influence of boreal summer monsoon intraseasonal oscillations on the occurrences of Marine Heatwave events over the North Bay of Bengal

Moulik Mandal[1] · Gopinadh Konda[2] · Naresh Krishna Vissa[1] · Jasti S. Chowdary[2]

Abstract

In the present study, the properties of Marine Heatwave (MHW) events over the North Bay of Bengal (BoB) are investigated during the boreal summer monsoon season. In recent decades (2001–2021), an increase in frequency and duration of MHW events are depicted, prominently after 2010. This accelerated trend in MHW events duration is primarily driven by the rapid ocean warming and is a great concern for the scientific as well as fisheries communities. Tropical intraseasonal oscillations are one of the dominant modes that control the oceanic and atmospheric processes. Here, for the first time, we have investigated the role of northward propagating monsoon intraseasonal oscillations (MISO) on the occurrences of MHW events over the north BoB during the boreal summer (monsoon season). It is found that during the break phases of MISO, enhanced shortwave radiation due to clear sky conditions triggers the MHW events. In addition, shallow mixed layer depth (MLD) also mostly favours the occurrences of MHW events over the north BoB during the break phases of MISO. However, during the active phases of MISO, negative sea surface temperature (SST) anomalies, and fewer MHW events are depicted over the north BoB. This strong relationship between shallow MLD and the occurrences of MHW events primarily indicates the connection of regional air-sea heat flux in driving the MHW events over the north BoB. The consequences of MHW events on socioeconomic status are also projected to be extensive, serious, and persistent throughout the twenty-first century.

Keywords Marine heatwaves · Boreal summer monsoon · Monsoon intraseasonal oscillations

1 Introduction

Marine Heatwaves (MHW) events are mainly discrete, prolonged, and extremely warm water events over a particular region of the ocean for continuous 5 days and more (e.g., Pearce 2011; Hobday et al. 2016; Holbrook et al. 2019). The 'MHW' term was first used to understand an extreme unprecedented warming event, called "Ningaloo Niño" which was first observed over the southeast Indian Ocean (IO) off the west coast of Australia during the peak of the La Niña event (2010–2011) (Feng et al. 2013; Chatterjee et al. 2022). In recent decades, MHW events have been observed in every ocean basin with an increasing trend in the annual mean MHW events frequency and duration (e.g., Hu et al. 2020; Huang et al. 2021a, b). Carvalho et al. (2021) linked underlying physical processes responsible for the MHW events in the Bering Sea with the neighbouring climatic patterns such as the teleconnections between the Pacific Ocean and the Arctic, sea ice extent, and adjacent air temperature. Recently, a study by Mohamed et al. (2022) mentioned that the Eastern Atlantic Pattern (EAP) is primarily responsible for the modulation of MHW events over the Barents Sea. Other recent events include—the unprecedented 2011 Western Australia Ningaloo Niño (Pearce and Feng 2013), the 2012 Northwest Atlantic MHW events (e.g., Mills et al. 2013; Chen et al. 2014), 2012 and 2015 Mediterranean Sea MHW events (e.g., Dayan et al. 2023), the 2013/14 western South Atlantic and 2017 South-Western Atlantic MHW events (e.g., Manta et al. 2018; Brauko et al. 2020), the persistent 2014–2016 "Blob" in the North Pacific (e.g., Di Lorenzo and Mantua 2016; Scannell et al. 2016),

✉ Naresh Krishna Vissa
vissan@nitrkl.ac.in; vissanaresh@gmail.com

1 Department of Earth and Atmospheric Sciences, National Institute of Technology Rourkela, Dist: Sundargarh, Rourkela, Odisha 769008, India

2 Ministry of Earth Sciences, Indian Institute of Tropical Meteorology, Pune 411008, India

the Tasman Sea MHW events in 2015/16 (e.g., Oliver et al. 2017) and 2017/18 (e.g., Salinger et al. 2019), the 2015/16 MHW events spanning over the south-eastern tropical IO (e.g., Benthuysen et al. 2018), and 2010, 2016, and 2020 north IO MHW events (e.g., Chatterjee et al. 2022) leading to the rapid change of ocean biogeochemistry.

With the rising global ocean temperatures, extreme weather events such as MHW events over the global oceans are projected to become more intense and frequent in recent decades (IPCC 2023). Xu et al. (2022) observed an increasing trend of MHW events without significant changes in the sea surface temperature (SST) variability and they have attributed to global warming-induced climate extremes. Pietri et al. (2020) showed that MHW events along the Peruvian coast can sustain even in the upwelling regions by addressing the role of local i.e., wind stress, heat fluxes, and remote i.e., equatorial wave activity. Holbrook et al. (2019) made a detailed assessment of MHW events and their drivers, and their findings suggest that different phases of known climate modes such as El Niño-Southern Oscillation (ENSO), Indian Ocean Dipole (IOD), Southern Annular Mode (SAM), and North Atlantic Oscillation (NAO) are predominantly enhancing or suppressing the livelihoods of MHW events throughout the global oceans. On the other hand, MHW events have different driving mechanisms depending on the local air-sea coupling (e.g., Du et al. 2009), advection, and heat transport by eddies (e.g., Gulakaram et al. 2023; Wyatt et al. 2023), atmospheric-oceanic pre-conditions (e.g., Saranya et al. 2022), oceanic circulations, and remote climate teleconnections (e.g., Holbrook et al. 2019). Among all the factors, advection and oceanic circulations both are playing a vital role in driving the deepest as well as prolonged MHW events (Elzahaby et al. 2021). Stratification and local winds are also crucial factors in driving the subsurface MHW events (e.g., Schaeffer and Roughan 2017). MHW events have devastating impacts on the marine ecosystem such as coral bleaching (e.g., Krishnan et al. 2011; Zinke et al. 2015; Patterson Edward et al. 2018; Wyatt et al. 2023), widespread harmful algal blooms (e.g., Takagi et al. 2022; Dodrill et al. 2023), reduction in seagrass meadows (Aoki et al. 2021). Few studies have shown that MHW events can impose severe threats to the marine environment including the mass mortality of zoo planktivorous seabirds (e.g. Jones et al. 2018). The marine phytoplankton biomass (chlorophyll) is very important as they regulate some major biogeochemical processes e.g., carbon uptake and transport over the ocean, forming the base of the aquatic food chain (Le Grix et al. 2021). MHW events also affect the Chlorophyll-*a* (Chl-*a*) concentration levels along the coastal regions (e.g., Hamdeno et al. 2022) leading to a reduction in primary production over the ocean (Chiswell and Sutton 2020). MHW events have significant impacts on economic species such as coastal fisheries and aquaculture (e.g., Mills et al. 2013; Cheung and Frölicher

2020; Habibullah et al. 2023). Recently, Wang et al. (2023) have shown that MHW events have changed the upwelling structure in the biologically productive southern hemisphere's eastern boundary upwelling systems (Humboldt and Benguela current systems) which further impacted the evolution of potential fishery zones. Despite the devastating ecological impacts of MHW events beneath the sea, very few studies have attempted to investigate the temperature extremes below the surface i.e., in the sub-surface.

Many studies have shown that there is a significant increase in background SST over the Tropical Indian Ocean (TIO) and adjacent basins in recent decades (e.g., Du et al. 2009; Zhang et al. 2017; Han et al. 2021; Li et al. 2022). According to Holbrook et al. (2019), teleconnections of the IOD via the Indian Ocean Basin (IOB) wide mode and ENSO are mainly responsible for the longer duration of MHW events over the IO. They also identified that the increasing trend in MHW events days' percentage over TIO is strongly influenced by the positive Dipole Mode Index (DMI) and negative NAO mode index. Saranya et al. (2022) analyzed the role of varying atmospheric-oceanic conditions before the genesis as well as after the evolution of MHW events over two different regions—the Western Indian Ocean (WIO) and the Bay of Bengal (BoB). They have found an increase in the annual and seasonal trend in MHW events' frequency over the above-mentioned two regions respectively for the period of 37 years (1982–2018). Further, they have identified that there is a strong relationship between MHW events over the north BoB and a significant increment in the boreal summer monsoon rainfall amount over southern peninsular India, whereas dry conditions over central India. On the other hand, IOB-wide mode via the decaying phases of El Niño is mainly responsible for the longer duration of MHW events over the Arabian Sea (AS) (Chatterjee et al. 2022). Albert et al. (2023) showed that during the premonsoon season, surface heat fluxes are mainly responsible for the higher SSTs over the AS. Similarly, Qi et al. (2022) showed that positive sea surface height anomaly associated with downwelling Rossby waves which are propagating westward, modulated by equatorial easterly winds, plays a vital role as one of the most prominent drivers of the MHW events over the western equatorial IO by weakening the upwelling. Recently, Lin et al. (2023) revealed that strong seasonal variability in the frequency of MHW events over the BoB is mainly induced by El Niño events. In that scenario, quantification of the possible drivers of MHW events is one of the most important challenges for the scientific community.

During the boreal summer monsoon season (June, July, August, and September), the North Indian Ocean (NIO) is very crucial as it supports high marine productivity (e.g., Roxy et al. 2016; Gao et al. 2022), and also exhibits strong intraseasonal and interannual SST variability (e.g., Roxy

and Tanimoto 2007; Singh and Dasgupta 2017; Konda and Vissa 2021). However, the spatial variability in the rainfall amount over India and surrounding regions is also significant as a response to the SST variability during the boreal summer monsoon season over the BoB (e.g., Roxy 2014). Hsu et al. (2017) performed a detailed analysis to understand the influence of Boreal Summer Intraseasonal Oscillation (BSISO) on atmospheric heatwaves over central India but very little attention has been paid to exploring the connection between intraseasonal oscillation and the occurrences of MHW events. On the other hand, Holbrook et al. (2019) mentioned on their study that regional air-sea coupling, sea level pressure, air-sea heat flux, and advection particularly drive MHW events over the BoB. Few studies have also quantified the MHW events over the BoB with a detailed analysis in terms of frequency, intensity, and spatial variability (e.g., Saranya et al. 2022; Gao et al. 2022; Lin et al. 2023). However, in the recent warming scenario, identifying the actual drivers of MHW events and understanding their role is toward predicting this extreme event accurately, is the topic of interest for the scientific community. To accomplish it, the present study has explored the role of monsoon intraseasonal oscillation (MISO) in driving the MHW events within the study region (80°–95° E and 15° N – 23° N) over BoB during the boreal summer monsoon season from 1982-2021. A shallow surface mixed layer (SML) results in more MHW events - classified as air-sea heat flux-driven and less classified as advection, similarly a deep estimate of SML produces the opposite pattern (Elzahaby et al. 2022). However, over the BoB, the amount of freshwater influx obtained directly from the precipitation and indirectly from the major Indian rivers' runoff, especially during the boreal summer monsoon season, distinguish the BoB from the rest of the world's oceans – mainly contributes to the formation of a thick barrier layer and significant saline stratification in the upper layers of the BoB (e.g., Vissa et al. 2013; George et al. 2019). This strong salinity stratification prevents heat from mixing vertically, as a result maintaining warm SSTs over the BoB which further contributes to the higher climatological rainfall over the BoB (e.g., Krishnamohan et al. 2019). Therefore, the present study has also examined the composite evolution of the mixed layer depth (MLD) anomaly during the MHW events over the BoB in addition to that of the MISO impacts.

Section 2 describes the datasets (Sect. 2.1) and the methodology (Sect. 2.2) that we have used in the present study. In the result and discussions section, Sect. 3.1 shows the seasonal SST trend per decade over the NIO from 1982 to 2021. The Sect. 3.2 performs the frequency analysis of MHW events during the boreal summer monsoon season over the north BoB whereas Sect. 3.3 addresses the role of ocean-atmospheric interactions in the modulation of higher SST during the MHW events over the north BoB. However,

in Sect. 4—the role of MISO in driving the MHW events over the north BoB during the boreal summer monsoon season, Sect. 4.1 mainly focuses on the influence of different MISO phases on the SST variability over the north BoB during the boreal summer monsoon as well as during the MHW events. On the other hand, a statistical analysis is presented in Sect. 4.2 for understanding the relationship between shallower mixed layer depth (MLD) and enhanced shortwave radiation due to the clear sky conditions in the break phases of the MISO with the occurrences of MHW events over the north BoB.

2 Data and methodology

2.1 Data

Identification and quantification of the MHW events within the study region over BoB are accomplished by using daily US National Oceanic and Atmospheric Administration (NOAA) Optimum Interpolation SST (OISST) v2.1 data sets with a spatial resolution of 0.25° × 0.25°, for the 40 years (1982–2021) (Reynolds et al. 2007; Huang et al. 2021a, b). Further, the high resolution (0.25° × 0.25°) monthly mean values of SST, obtained from NOAA OISST v2.1, are used to analyze the seasonal as well as annual SST trend over the NIO for the same study period of 40 years (Banzon et al. 2016). In addition, also used the Mean surface net short-wave radiation flux (SWR) and Mean surface latent heat flux (LHF), Air temperature (AT) at 2 m height, and Total Cloud Cover (TCC), obtained from the European Centre for Medium-Range Weather Forecasts (ECMWF) atmospheric reanalysis (ERA5) from 1982 to 2021 with spatial resolution 0.25° × 0.25° to study the impacts of MHW events on the ocean-atmosphere system (Hersbach et al. 2020). The daily gridded dataset of Sea Surface Height anomaly (SSHA) and ocean mixed layer depth (MLD) both are obtained from the Copernicus Marine Environment Monitoring Service (CMEMS) on a spatial resolution of 0.25° × 0.25° and 1/12° × 1/12° respectively, available from 1993 to 2020 and is used to understand the induction of ocean Equatorial (Rossby and Kelvin) waves and ocean mixing in driving the MHW events during the boreal summer monsoon season over north BoB (Pascual et al. 2006). The daily Zonal Wind Stress (ZWS), Meridional Wind Stress (MWS), Net Heat Flux (NHF), and Wind Speed (WS) data sets are obtained from the TropFlux project of the Indian National Centre for Ocean Information Services (INCOIS) with resolution 1° × 1° for the period of 1982–2018 (Praveen Kumar et al. 2012, 2013). For further analysis, the best track datasets containing the cyclonic disturbances days (including both the depressions and tropical cyclones days) are obtained from the Regional Specialized Meteorological Centre, Indian Meteorological Department

(IMD) to identify the cyclonic disturbances' days over the north BoB (Mohapatra et al. 2013).

During the boreal summer monsoon season, the location and strength of the intraseasonal oscillation are evaluated from the extended empirical orthogonal function (EOF) index i.e. MISO index developed by Suhas et al. (2013) by using unfiltered daily anomalies of the rainfall, averaged over the longitudinal region between 60.5° and 95.5° E and is obtained from the Indian Institute of Tropical Meteorology (IITM). The mass concentration of chlorophyll-*a* in seawater is derived from Moderate Resolution Imaging Spectroradiometer (MODIS)—Aqua Level-3 (L3) mapped data from NASA Ocean Color (OC) web, having a spatial resolution of 9 km to highlight the response of marine phytoplankton biomass to the MHW events occurrence in the coastal water (Noh et al. 2022). The daily dataset of SST has been used on a particular grid (90° E and 15° N) over the study region. These daily datasets are obtained from the Research Moored Array for African-Asian-Australian Monsoon Analysis and Prediction (RAMA) buoy which is designed for exploring the role of the Indian Ocean during the boreal summer monsoon season. These in-situ observations for the study period of 14 years (2008–2021) during the boreal summer monsoon season are used to cross-validate the obtained results derived using satellite products (McPhaden et al. 2009).

2.2 Methodology

The present analysis uses the widely adopted hierarchical method to identify the MHW events, proposed by earlier studies (e.g., Hobday et al. 2016; Holbrook et al. 2019; Saranya et al. 2022). According to their studies if the daily SST derived from NOAA OI, is above the 90th percentile (T90) threshold value and persists for continuous 5 days and more, then this discrete, prolonged as well as anomalously warm event can be called an MHW event. If the gap between two MHW events with subsequent 5 days or more, is of 2 days or less, then these two events will be marked as a continuous single event (Hobday et al. 2016). In the present analysis, the T90 values of SST at each grid are calculated from the daily time series of SST by creating an 11-day window centered on that particular day of the year across all years from 1982 to 2021. This window of 11 days is considered for producing enough sample size at a daily timescale for estimating the T90 values (Saranya et al. 2022). The baseline daily climatology of SST within the climatology period (1982–2021) is calculated from the daily SSTs by using a 31-day moving average. Here, the moving average of 31 days is applied to derive a smoothed climatology which is only varying seasonally (Oliver et al. 2018; Sen Gupta et al. 2020). This is very important because day-to-day fluctuations in the SST values sometimes increase the baseline daily climatology and T90 values very high. A day-specific threshold for a

particular season allows for the identification of MHW days in all seasons of the year including the winter season. MHW events with large spatial extents are the most devastating than smaller ones (Oliver et al. 2018), so in addition to the above conditions, added one more condition—only considered those MHW events for the further analysis that at least crossed 1/4th of the total gridded area of the study region. The present analysis of detecting MHW days is finally accomplished by excluding all the cyclonic disturbances' days over the BoB from further analysis for the same periods. The present study also provided a flowchart diagram (Fig. 1) to summarize the method to detect the MHW events over the north BoB during the boreal summer monsoon seasons, discussed in this methodology section.

The Mann–Kendall (MK) trend test is used to assess the significance of the change in the monthly mean SST values over the NIO and Sen's slope method to estimate the rate of change in the SST per decade. To analyze the frequency of MHW events over the north BoB, the number of MHW events at each grid has been calculated seasonally from 1982
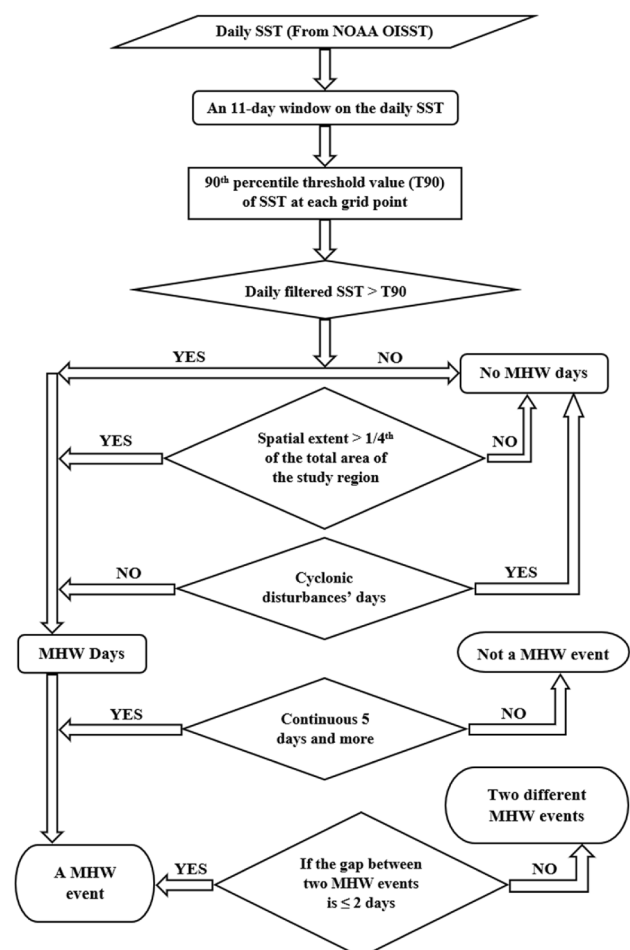

Fig. 1 Flowchart diagram to summarize the method to detect the MHW events over the north BoB

to 2021 (e.g., Qi et al. 2022; Saranya et al. 2022; Lin et al. 2023) and the yearly time series of the number and duration of MHW events (yearly total number of MHW days) from 1982 to 2021. To perform the trend analysis of the SST over north BoB, the area average of SST anomaly has been calculated over the north BoB during the boreal summer monsoon seasons and then a linear trend model is fit. The life cycle of MHW events is examined by normalizing the SST anomaly of the individual event from 0 to 1 and averaging for all the events (Wang et al. 2022). In addition, a composite analysis is performed for SST, SWR, TCC, SSHA, AT (2 m height), ZWS, NHF, and WS anomalies during the MHW days for understanding the dynamical and physical processes responsible for the MHW events over the north BoB.

The first two principal components of the extended EOF analysis – MISO1 and MISO2 indices, together reflect the evolution of the MISOs in the low-dimensional phase

$$\text{MISO Amplitude } = \sqrt{MISO1^2 + MISO2^2}$$

which may be greater than 1 or less than 1. If a MISO phase has an amplitude greater than 1, it implies that MISO is strong and significant. However, a composite analysis of the MLD anomaly during the MHW days has been performed to understand the dependency of MHW events over the north BoB either on air-sea heat flux or ocean heat advection. Further, a statistical analysis is performed to understand the combined role of shallower MLD and enhanced SWR due to MISO break phases in driving the MHW events over the north BoB during the boreal summer monsoon season. Here, the present analysis has considered the MISO amplitude

associated with break and active phases to have negative and positive values respectively. To understand the biogeochemical changes during the MHW events over the north BoB, a composite analysis of Chl-*a* is performed considering the MHW days. The significance of the composite analysis was examined at the 95% level of confidence using the conventional two-tailed Student's *t*-test.

3 Results and discussions

3.1 Seasonal SST trend over the North Indian Ocean

Oliver (2019) showed that the rising mean ocean temperature is the main driving factor for an increasing trend in the MHW durations over two-thirds of the global oceans during this satellite era. Over the NIO, the SST trends are evaluated using monthly SST data for the period of 40 years (1982–2021) during all the seasons and are shown in Fig. 2. The analysis reveals a significant warming trend over the NIO annually as well as seasonally. On the annual scale, warming is prominent over the north AS (Fig. 2a), whereas, during the boreal summer monsoon season, significant warming is seen over the north BoB also with the north AS (Fig. 2b). While during pre-monsoon and post-monsoon seasons, the north BoB experiences anomalous warming of ~ 0.15 °C per decade (Fig. 2c) and ~ 0.05 °C per decade (Fig. 2d) respectively, during boreal summer monsoon seasons the warming of more than 0.35 °C per decade is consistent over the north coast of BoB. On the other hand, during the winter seasons (January and February) of the northern
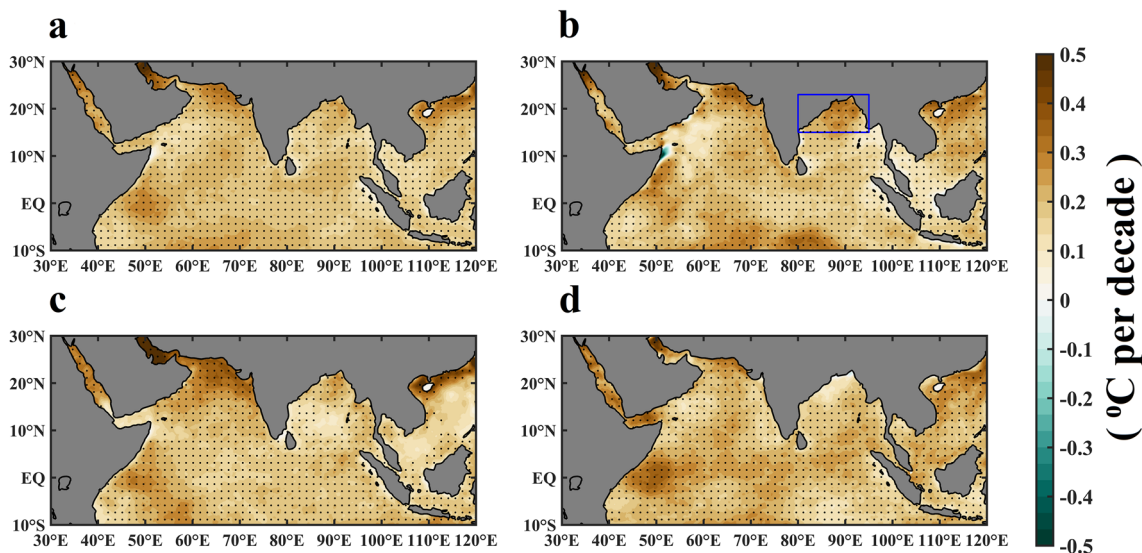

Fig. 2 Trends in SST (in °C) per decade for the period of 40 years (1982–2021) over the NIO for **a** annual, **b** summer monsoon, **c** pre-monsoon, and **d** post-monsoon season. Trend values that are significant at a 95% confidence level are indicated by stippling (black dots). The regions with grey shade in the figures indicate the land area. The blue rectangular box in (**b**) represents the study area over BoB

hemisphere, summer season takes place in the southern hemisphere and the southern hemisphere receives most of the insolation. So, the cooling of SST occurs over the north IO during the winter season (Fig. S1). Consequently, the trend in the number of MHW days during the winter seasons over the study region is also showing a negative trend (Fig. S3a).

Further, the thermodynamic structure of north BoB in the context of near-surface temperature (e.g., Goswami et al. 2022; Masud-Ul-Alam et al. 2022), salinity (e.g., Vinayachandran et al. 2002), circulations (e.g., Schott et al. 2009), cyclonic activity (e.g., Vissa et al. 2021; Rathore et al. 2022) and cyclone heat potential (e.g., Sadhuram et al. 2004), mesoscale eddies (e.g., Gulakaram et al. 2023), net freshwater influx – both river input and precipitation (e.g., Seo et al. 2009; Jana et al. 2015) play a vital role in influencing the regional air-sea interactions over micro to synoptic-scale systems. Hence, by recognizing the ecological as well as socioeconomic importance of north BoB the present analysis majorly focused on the north BoB (80°–95° E and 15°–23° N) and investigated the occurrence of extreme temperature events i.e., MHW events over that region during the boreal summer monsoon seasons.

3.2 Frequency analysis of MHW events over the north BoB

The spatial distribution of the 90th percentile threshold across the BoB shows that the T90 values are high over the north and west coast of BoB (Fig. 3a), which are approximately 0.5–1.5 °C higher than the climatological values over the region. Moreover, both the climatology and T90 values of SST during the boreal summer monsoon season are significantly higher over the north and west coast of BoB and the Andaman Sea regions. Most of the distribution of coral reefs over the BoB is located over the 3 regions, i.) Southwest of BoB (77°–83° E and 5°–12.5° N), ii.) Andaman

Sea (91°–100° E and 5°–14° N), and iii.) Northeast BoB (91°–95° E and 15.5°–21° N) (Lam et al. 2019). Interestingly, it is noticed that higher SST values are over the regions where the coral reefs' concentration is high (Gao et al. 2022). The frequency analysis of MHW events over the BoB during the boreal summer monsoon season showed a prominent increase in the frequency of MHW events of more than 0.9–1.05 events per year for the periods of 40 years over north and north-western parts of BoB (Fig. 3b). Particularly, the north BoB region has experienced a prominent increase in MHW events' frequency of more than 1.05 events per year.

Furthermore, trend analysis of SST anomaly (Fig. 4a) over the study region signifies an opposite trend in the recent 2 decades (2001–2021) than the previous one (1982-2000). This decadal trend analysis strongly implies the significant increment in SST over the north BoB in recent decades with the rate of the BoB warming compared to the previous one (e.g., Sridevi and Sarma 2021). The recent two decades have experienced more MHW events with an average value of 1.3 MHW events with ~ 23 MHW days per year compared to the previous one (0.5 events with ~ 7 MHW days per year) during the boreal summer monsoon seasons (Fig. 4b, c). The trend analysis in the number of MHW days further signifies that there is a decline in the number of MHW days during the winter seasons whereas an increasing trend is prominent in the number of MHW days during both the pre-monsoon and post-monsoon seasons over the north BoB (Fig. S3). The north BoB experienced intense MHW events in terms of MHW events intensity in the years 2010, 2014, 2016, 2020, and 2021 but the special extent of MHW events during the boreal summer monsoon season of 2014, 2017, 2018, 2020, and 2021 is more than 0.80 Mkm^2 for consecutive 2-7 days, with a minimum of 0.21 Mkm^2 in the year 2012. Whereas the maximum area covered by the MHW
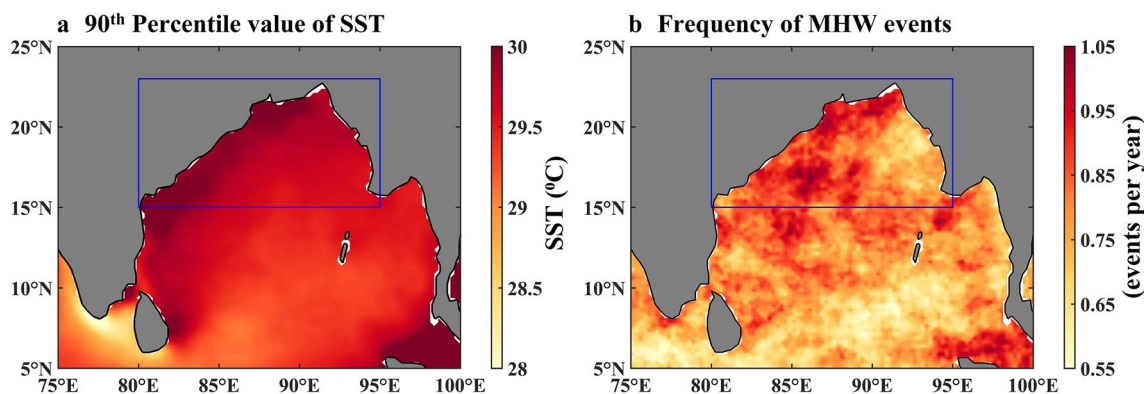

Fig. 3 **a** 90th percentile of daily SST (in °C) and **b** Mean frequency of MHW events for the period of 40 years (1982–2021) during the boreal summer monsoon season over the BoB. The regions with grey shade in both figures indicate the land area and the blue rectangular box represents the study area over BoB

Fig. 4 **a** Linear trend in SST anomaly (in °C), **b** the yearly number of MHW events, **c** yearly MHW events' durations, and d) Composite series of SST anomalies (in °C) for all MHW events during the boreal summer monsoon season over north BoB from 1982 to 2021
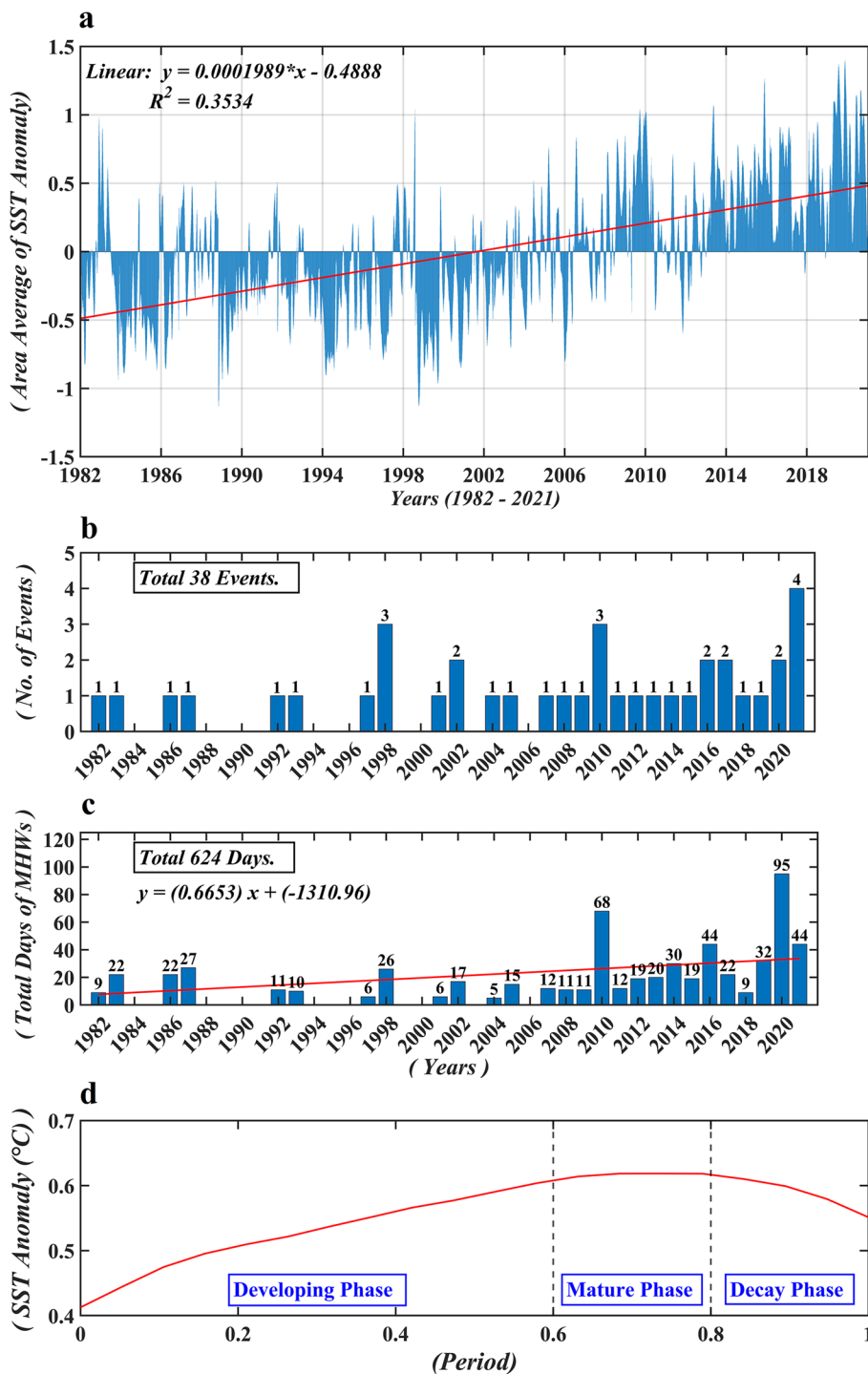
events is 0.84 Mkm² in the year 2020 and 2021. In the case of a high number of MHW events in the year 2020, the oceanic downwelling Rossby waves and thermocline warming, induced by extreme 2019 positive IOD event leading to the sea surface warming via thermocline-SST feedback during late 2019 to early 2020 over the southwest TIO and modulate the second SST warming over the north

IO during the boreal summer monsoon season (Zhang and Du 2021; Zhou et al. 2021; Cai et al. 2022; Cao et al. 2022).A composite of area-averaged SST anomaly was produced from each MHW event case and projected along a time axis starting from 0 to 1 to understand the three stages of MHW events' life cycle's progression – developing phase, mature phase, and decay phase (Figure 4d) (Wang et al. 2022).

3.3 Role of atmosphere–ocean interactions in the SST variability over north BoB during the MHW events

The frequent occurrence of MHW events over the BoB exhibits a teleconnection between climate modes and basin-wide warming (e.g., Holbrook et al. 2019; Saranya et al. 2022). Similarly, the relationship between the occurrences of MHW events and the atmosphere-ocean interactions strongly indicates the importance of regional forcing to be considered in the evolution of MHW events. The composite analysis of the atmospheric and ocean parameters during the MHW days over BoB provides extensive pictures of the mechanism behind the MHW event's genesis, persistence, and evolution with time. The spatial composite of SST anomaly during the MHW days for boreal summer monsoon seasons is shown in Fig. 5a and a higher SST anomaly is consistent over the whole study region during MHW events. It is noticed that the persistence of higher SST during MHW events over the north BoB is linked with enhanced SWR due to less cloud cover than usual. The positive SSHA, a negative anomaly of wind stress, a reduction in the wind speed, and comparatively higher air temperature over the

land surrounding and within the study region have played significant role in the increment of SST. Further, it is identified that SWR anomalies showed a dipole pattern during MHW events with positive anomalies over the north BoB and negative values over the south and central BoB (Fig. 5b). Further, the composite anomaly of TCC indicates less cloud cover over the north BoB and surrounding regions during the MHW events (Fig. 5c). This less cloudy condition than usual during boreal summer monsoon season is crucial in driving the background SST warming and the primary cause for the SWR variability over north BoB. Meanwhile, positive net heat flux (NHF) anomaly (Fig. 6c) and negative wind speed anomaly (Fig. 6d) over the study area during the MHW days have provided favorable conditions for the genesis and persistence of MHW events. A decrease in wind speed results in a decrease in ocean surface evaporation, which further reduces the effect of evaporative cooling and the release of upward LHF from the ocean surface.

The positive values of SSHA coincide with the positive SST anomaly in the same region over the BoB where the positive SWR anomaly is evident (Fig. 5d). This implies that the oceanic planetary waves modulated by anomalous equatorial winds converge surface warm water over there (Qi
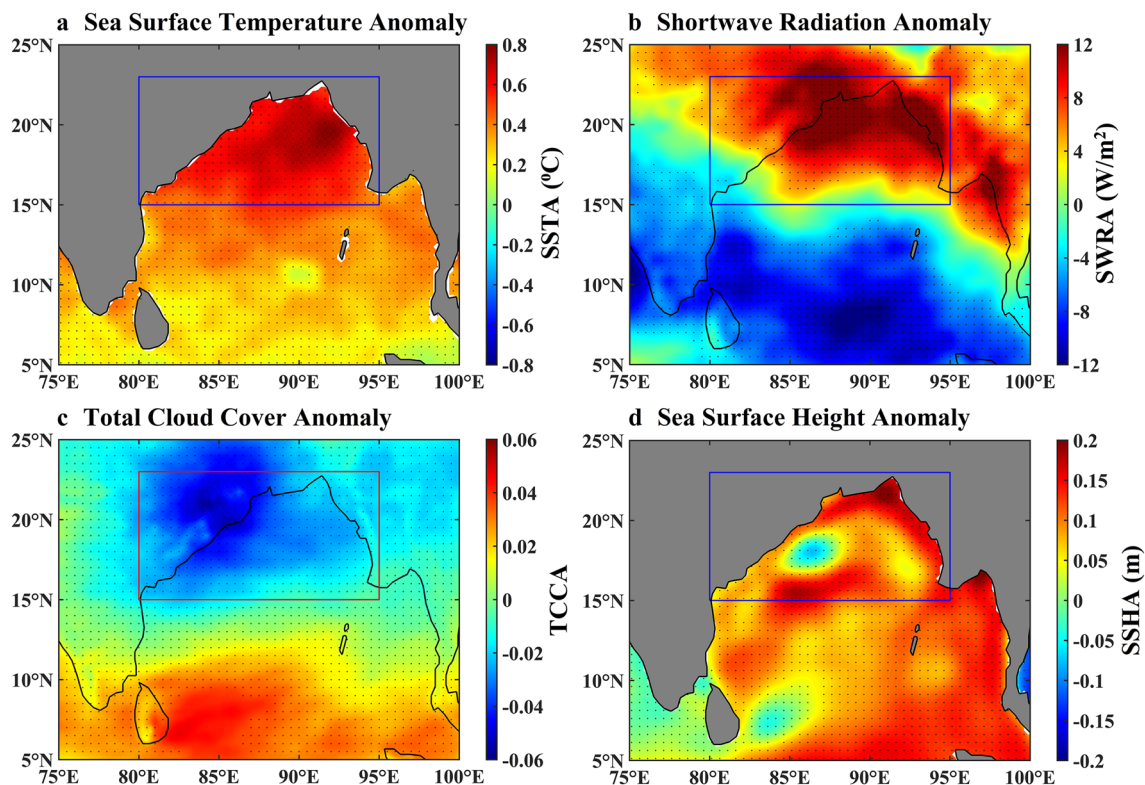

Fig. 5 The composite analysis of **a** Sea Surface Temperature Anomaly (SSTA in °C), **b** Shortwave Radiation Anomaly (SWRA in W/m^2), **c** Total Cloud Cover Anomaly (TCCA), d) Sea Surface Height Anomaly (SSHA in m) over the BoB during MHW days for the period of 1982–2021. The regions with grey shade in figures (**a**, **d**) indicate the land area. The blue and red rectangular boxes represent the study area over BoB. Anomaly values that are significant at a 95% confidence level are indicated by stippling (black dots)
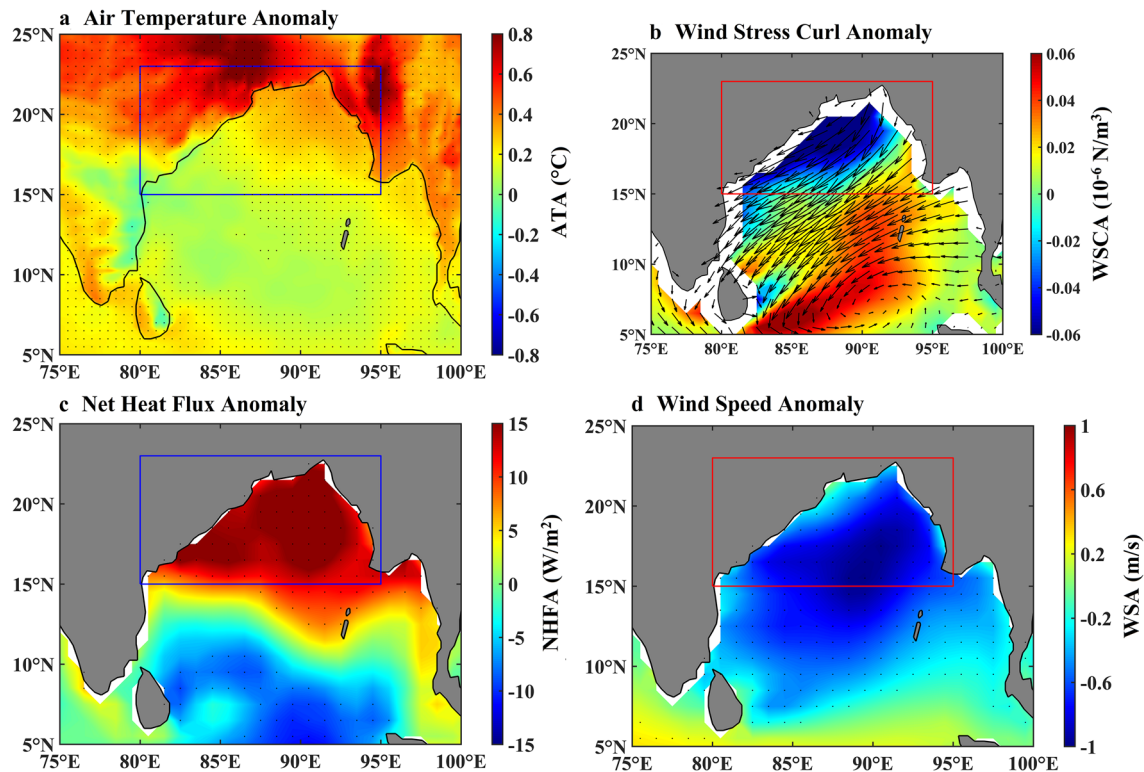
Fig. 6 The composite analysis of **a** Air Temperature Anomaly (ATA in °C), **b** Wind Stress Curl Anomaly (WSCA in 10^{-6} N/m³; shading) and surface wind stress anomaly (N/m²; vector), **c** Net Heat Flux Anomaly (NHFA in W/m²) **d** Wind Speed Anomaly (WSA in m/s) over the BoB during MHW days for the period of 1982–2021. The regions with grey shade in figure (**b–d**) indicate the land area. The blue and red rectangular boxes represent the study area over the BoB. Anomaly values that are significant at a 95% confidence level are indicated by stippling (black dots)

et al. 2022). The convergence of upper-ocean warm water over the north BoB is responsible for the higher SST and also favours the persistence of MHW events on the ocean surface. Both the oceanic waves—Kelvin and Rossby are responsible for the thermocline variation over the ocean (e.g., Xie et al. 2002; Vinayachandran et al. 2021; Qi et al. 2022). The present study further found that SSHA has a maximum value of more than 0.2 m over the north and eastern BoB. On the other hand, positive values of SSHA are identified over most of the regions of BoB during MHW days in the boreal summer monsoon season, implying the convergence of the surface warm water over these regions and deepening the thermocline, modulated by the oceanic planetary waves—the coastally trapped downwelling Kelvin waves and reflected downwelling Rossby waves over the central BoB (e.g., Rao et al. 2010). Due to the pilling of the warm water, the sea level rises, resulting in the deepening of the thermocline. The positive value of SSHA over the north and eastern coast of BoB is comparatively higher than the western coast, it signifies that besides the positive value of SSHA, the thermocline variability also plays a crucial role during the life cycle of MHW events. Furthermore, the presence of cyclonic and anticyclonic mesoscale circulations

are inherent features of the western Bay of Bengal (BoB) along the pathways of East India Coastal Current (EICC) (e.g., Vinayachandran 2005; Durand et al. 2009). Similar kind of features are also reported by Gulakaram et al. (2018) during the active boreal summer monsoon years. However, over the BoB negative SSHA anomalies (associated with cyclonic eddies) might not be associated with the negative SST anomalies (e.g., Gulakaram et al. 2023).

During the MHW days, a high value of positive air temperature anomaly at a 2 m height is seen on the surrounding land over the northeastern and northwestern parts of the study region (Fig. 6a). This comparatively higher air temperature during MHW days suggests that there might be a chance of shifting atmospheric heatwaves into the ocean or the atmospheric heatwaves creating favorable conditions for the genesis of MHW events or there is a possibility of co-occurrence of atmospheric as well as oceanic heatwaves for the same periods (Salinger et al. 2019; Behr et al. 2021; Cook et al. 2022; Pathmeswaran et al. 2022; Aboelkhair et al. 2023). On the other hand, negative values of wind stress curl anomaly are found over the north BoB during the MHW days in the boreal summer monsoon seasons (Fig. 6b). Furthermore, the wind stress (vector) during

the MHW days is found to be directed with the west coast of BoB in a way that it points to the coastal region on the right in the northern hemisphere, this signifies coastal downwelling associated with the Ekman Transport (ET) which is directed towards the west coast of BoB. Further this coastal downwelling is favorable for temperature intensification in the subsurface layers over the study region and supported the longer persistence of MHW events during boreal summer monsoon seasons.

4 Role of MISO in driving the MHW events

4.1 Influence of MISO on the SST Variability over the North BoB

The variability of southwest monsoon on the sub-seasonal timescales is associated with active as well as break phases of monsoon rainfall (e.g., Rajeevan et al. 2010; Pai et al. 2016). This variability in the convective activity during the boreal summer monsoon season associated with the wet and dry spells of rainfall is mainly modulated by the 30–60 days of northward propagating oscillations, coupled with large-scale circulation and convection, called MISO (Deshpande and Goswami 2014). The monsoon intraseasonal oscillation is starting from peninsular India (Phase 1), reaching north India and the Himalayan foothills at Phases 4 and 5, and it is ended up over Peninsular India at Phase 8 (Fig. 9) (Suhas et al. 2013). The cloud covers associated with the convection during the boreal summer monsoon seasons fluctuate

the incoming rate of solar radiation which is reaching to the surface through the atmosphere. The active phases of MISO are associated with convection i.e., more cloud covers than usual which will further reduce the amount of incoming SWR reaching the surface, in turn, will reduce the SST values. But during MISO break phases, the positive value of SST anomalies will be over the same region due to enhanced SWR (e.g., Konda and Vissa 2019).

The composite SST anomalies for all the boreal summer monsoon days when the MISO amplitudes are greater than 1 from 1998 to 2020 associated with the different phases of MISO are shown in Fig. 7 and it is noticed that the spatial variability of SST over the BoB is considerably impacted by the different phases of MISO. The positive values of SST anomaly are situated over the north BoB during the MISO phases 1, 2, 3, 7, and 8 whereas the negative SST anomalies are mainly associated with phases 4, 5, and 6. It is identified that MISO phases 3 and 7 are the transition phases (Fig. 7c, g) (Konda and Vissa 2019). Phase 3 has shown a transition from the higher SST anomalies in Phase 2 to lower SST anomalies in Phase 3 over the study region, whereas, Phase 7 has witnessed the transition from Phase 6 changing from a negative SST anomaly to a positive SST anomaly in Phase 7. The spatial variations of the composite analysis of SST anomalies for all the boreal summer monsoon days from 1998 to 2020 irrespective of MISO amplitudes associated with MISO phases has shown a similar pattern where MISO phases 1, 2, and 8 have displayed a comparatively higher value of SST anomaly than the other five phases and phases 3 and 7 of MISO are the transition phases (Fig. S4).
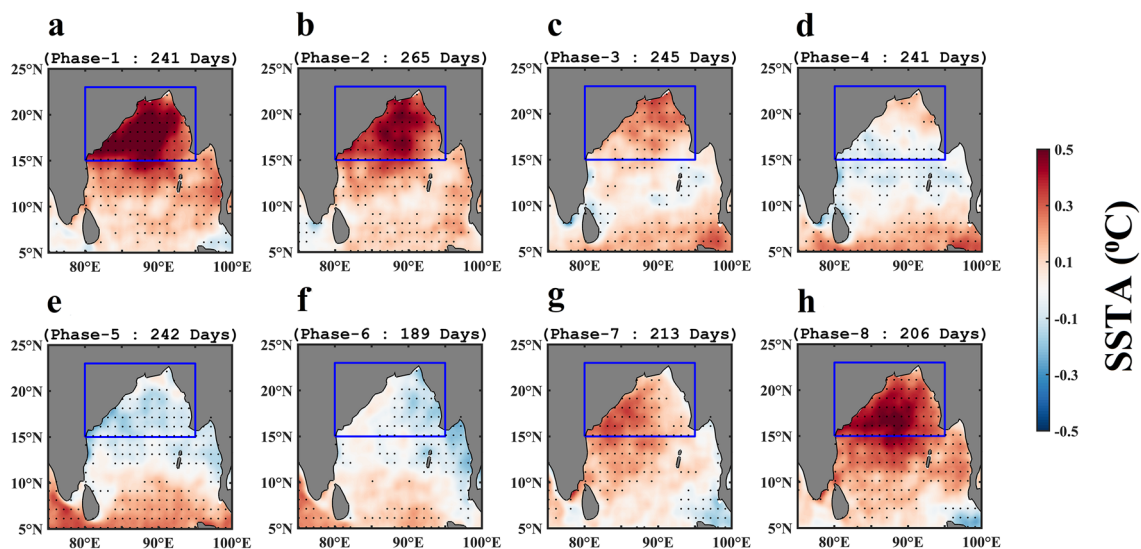

Fig. 7 The composite SST anomalies (in °C) in different phases of MISO, associated with all the boreal summer monsoon days when MISO amplitudes are greater than 1 from 1998 to 2020. The regions with grey shade in the figure indicate the land area. The blue rectangular boxes represent the study area over BoB. Anomaly values that are significant at a 95% confidence level are indicated by stippling (black dots)

The composite analysis of SST anomalies for MHW days when MISO amplitudes are greater than 1 has shown that SST anomalies are quite high over the study region for almost all the MISO phases except Phase 5 (Fig. 8). The number of MHW days associated with different MISO phases has shown that phases 1, 2, and 8 witnessed halves of the MHW days over north BoB when MISO is strong, indicating the presence of favorable conditions for the occurrence of more MHW events, mainly in these MISO phases. The composite SST anomalies associated with different MISO phases for all the MHW days irrespective of MISO amplitudes during the boreal summer monsoon seasons for the period of 1998-2020, displayed that MISO phases 1, 2, 3, and 8 exhibits comparatively higher SST anomaly than the other four phases (Fig. S5). The study region during these MISO phases has shown a higher SST anomaly value of more than 0.9 °C, persisting for all the MHW days, whereas

the spatial distribution of SST anomalies during MISO phases 4, 5, 6, and 7 showed a consistent range of SST anomaly nearly 0.5 °C. The number of MHW days dropped to 52 in Phase 3 from the number 94 MHW days in Phase 2, almost half and the number of MHW days stepped up to the number of 51 in Phase 7 from 21 MHW days in Phase 6.

The mean of SST anomalies over the north BoB during different phases of MISO for all and MHW days with amplitudes greater than 1 and for all amplitudes are given in Table 1. During the active phases, weak as well as negative SST anomalies are seen for all the days with amplitudes greater than 1 and for all MISO amplitudes. However, positive SST anomalies are depicted during the break phases of MISO. For MHW days, positive SST anomalies are evident during all the phases, whereas, prominent for the break phases of MISO with amplitudes greater than 1. Here also, Phase 7 has shown a transition from a decaying
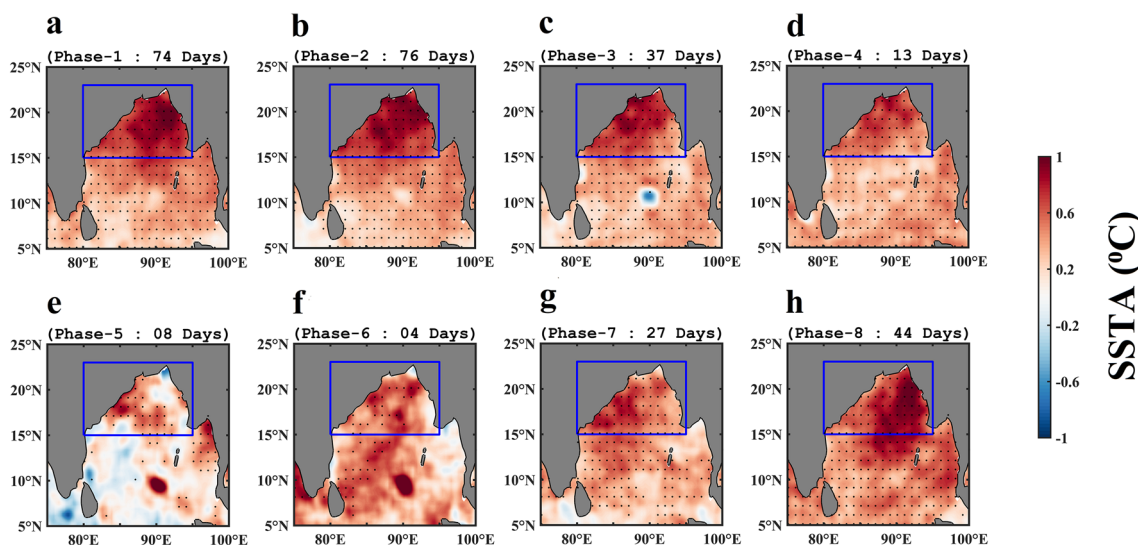

Fig. 8 The composite SST anomalies (in °C) in different phases of MISO, associated with the MHW days during the boreal summer monsoon seasons when MISO Amplitudes are greater than 1 from 1998 to 2020. The regions with grey shade in the figure indicate the land area. The blue rectangular boxes represent the study area over BoB. Anomaly values that are significant at a 95% confidence level are indicated by stippling (black dots)

Table 1 The mean of SST anomalies averaged over the study region for different phases of MISO during the boreal summer monsoon season (1998–2020) associated with the 4 cases mentioned below

	Days	MISO Amplitudes	(MISO Phases)							
			1	2	3	4	5	6	7	8
Sea Surface Temperature	For All the Days	*Case I*: For All MISO Amplitudes	0.37	0.33	0.17	0.05	− 0.05	− 0.08	0.09	0.29
		Case II: For MISO Amplitudes > 1	0.41	0.36	0.21	0.04	− 0.07	− 0.06	0.15	0.33
	For the MHW Days	*Case III*: For All MISO Amplitudes	0.71	0.76	0.67	0.54	0.46	0.45	0.47	0.61
		Case IV: For MISO Amplitudes > 1	0.78	0.80	0.69	0.60	0.21	0.43	0.51	0.73

trend coming from Phase 3. Even in cases I and II, Phase 7 have witnessed a transition from the negative mean values present in MISO phases 5 and 6 to the positive values of SST anomaly. Whereas the mean SST anomaly has dropped to almost half in phase 3 for cases I and II from phase 2 and for cases III and IV, phase 3 showed an alternation from an increasing trend to a decreasing trend of mean SST anomaly. As a consequence, MISO phases 1, 2, 7, and 8 have been considered as break phases, and MISO phases 3, 4, 5, and 6 are the active phases over the north BoB during boreal summer monsoon season (e.g., Dey et al. 2022).

Active phases of MISO are associated with convection and extensive cloud cover, whereas break phases are coupled with a very small amount of cloud cover. That indicates north BoB received a sufficient SWR during the MISO break phases, warming the ocean surface. This warm SST further modulates the genesis and persistence of MHW events over the north BoB. Alternatively, incoming SWR during the active phases is insufficient for the modulation of SST, consequently, MHW days are significantly less during active MISO phases than during the break phases. Further, the percentage of occurrences of MHW events associated with different MISO phases is calculated and shown in Fig. 9. Analysis reveals that over the north BoB, a large percentage of MHW days of more than 69% are associated with

the break phases of MISO i.e., MISO phases 1, 2, 7, and 8, whereas, a less percentage of MHW days are seen during the active phases of MISO (MISO phases 3, 4, 5, and 6) irrespective of MISO amplitudes. However, when the MISO amplitudes are greater than 1, the percentage of MHW days associated with the MISO break phases is 78% but there also a very less percentage of MHW days are associated with MISO active phases over the north BoB during the boreal summer monsoon season.

4.2 Role of MLD and MISO break phases in driving the MHW events over the north BoB: a statistical analysis

The composite of MLD anomalies during MHW days from 1993 to 2020 showed that a shallower depth of mixed layer than usual is consistent over the north BoB up to 10° N, whereas over the south of the study region, there are positive MLD anomalies (Fig. 10). A dipole-like pattern associated with positive MLD anomalies over the southern BoB and negative over the northern BoB is apparent. Due to very less cloud cover and a reduction in the wind speed during the MHW days, a high amount of SWR heated the surface of the north BoB, as a result, the SST values are higher than normal, which led to the

Fig. 9 The Phase Diagram of MISO. Black boxes within the diagram and outside of the diagram indicate the phase and location of MISO respectively over India and the surrounding region. The red and blue boxes inside the diagram are showing the percentage of days associated with the conditions mentioned in the red and blue boxes respectively just the right side of the diagram
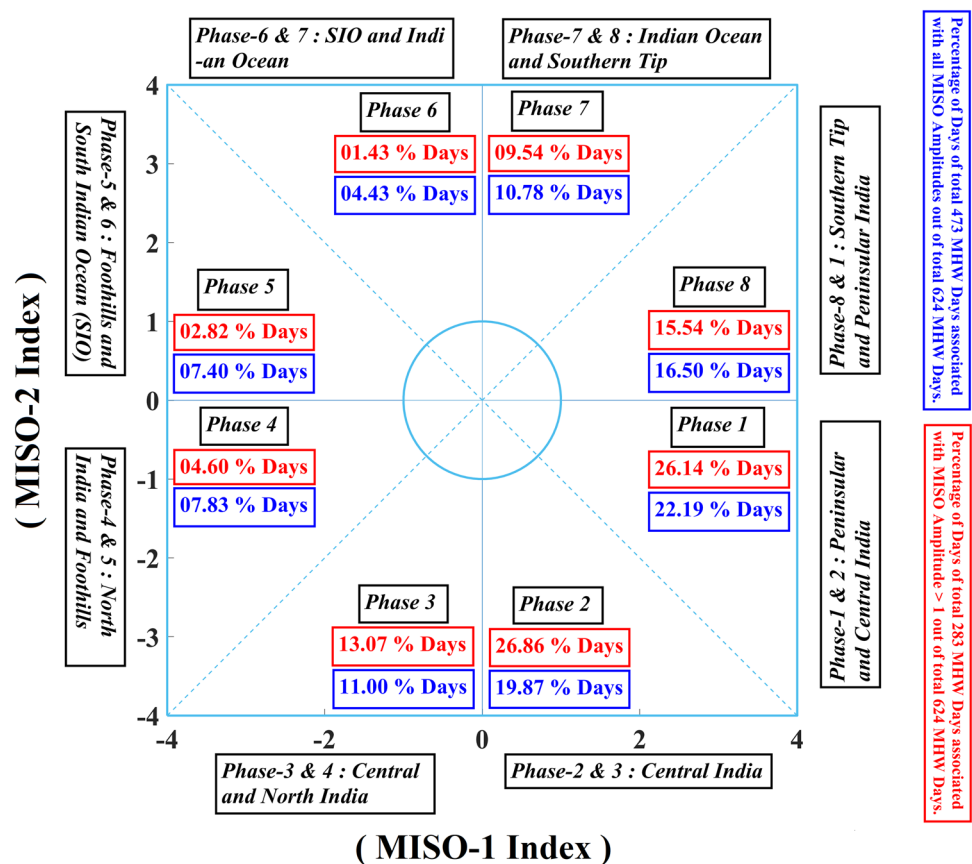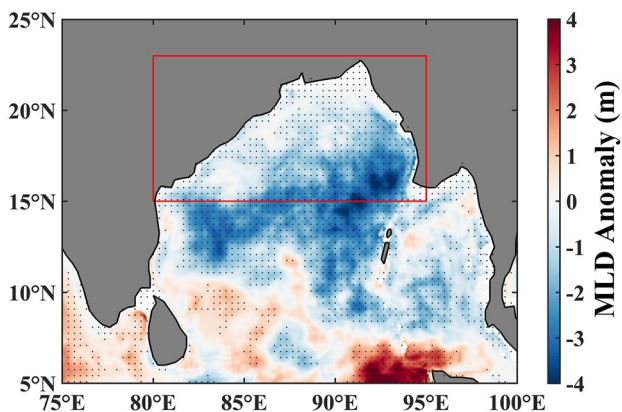
Fig. 10 Composite of Mixed Layer Depth Anomaly (MLD Anomaly, m) during MHW days in the boreal summer monsoon season from 1993 to 2020 over BoB. The regions with grey shade in the figure indicate the land area. The blue rectangular box represents the study area over BoB. Anomaly values that are significant at a 95% confidence level are indicated by stippling (black dots)

stratification and shallowing of the MLD (e.g., Prasanna et al. 2002). The shallowing of MLD further supports the MHW events over the north BoB, mainly associated with the higher contribution from the air-sea heat flux but less associated with the oceanic heat advection (e.g., Saranya et al. 2022). Elzahaby et al. (2021) showed that anomalous warming during the MHW events on average over

the Tasman Sea is mainly restricted to shallow MLD when driven by atmospheric forcing.

Further, a statistical analysis is performed to understand the combined role of shallow MLD and enhanced SWR associated with MISO break phases in the genesis and evolution of MHW events, as a primary driver of surface warming over the north BoB. The amplitudes associated with MISO break phases (phases 1, 2, 7, and 8) are chosen as a favorable condition for enhanced SWR, and amplitudes coupled with MISO active phases (phases 3, 4, 5, and 6) are associated with a less amount of insolation over the study region. The area average of MLD anomaly is computed over the study region and the scattered distribution of the area average of MLD anomaly values (1993-2020) and MISO amplitudes (1998–2020) associated with the MHW days (a total of 473 MHW days from 1998 to 2020) are shown in Fig. 11. Furthermore, the percentage of days associated with the 4 conditions—when both the MISO amplitudes and MLD anomaly values are positive; when MISO amplitudes > 0 but MLD anomaly values < 0; when both the MISO amplitudes and MLD anomaly values are negative; when MISO amplitudes < 0 but MLD anomaly values > 0 are computed respectively. Based on the previous analysis, it is clear that when both the values are negative it can generate the favorable background conditions for the genesis and persistence of MHW events than the other three. So, it is projected that more MHW days are associated with the case when both the
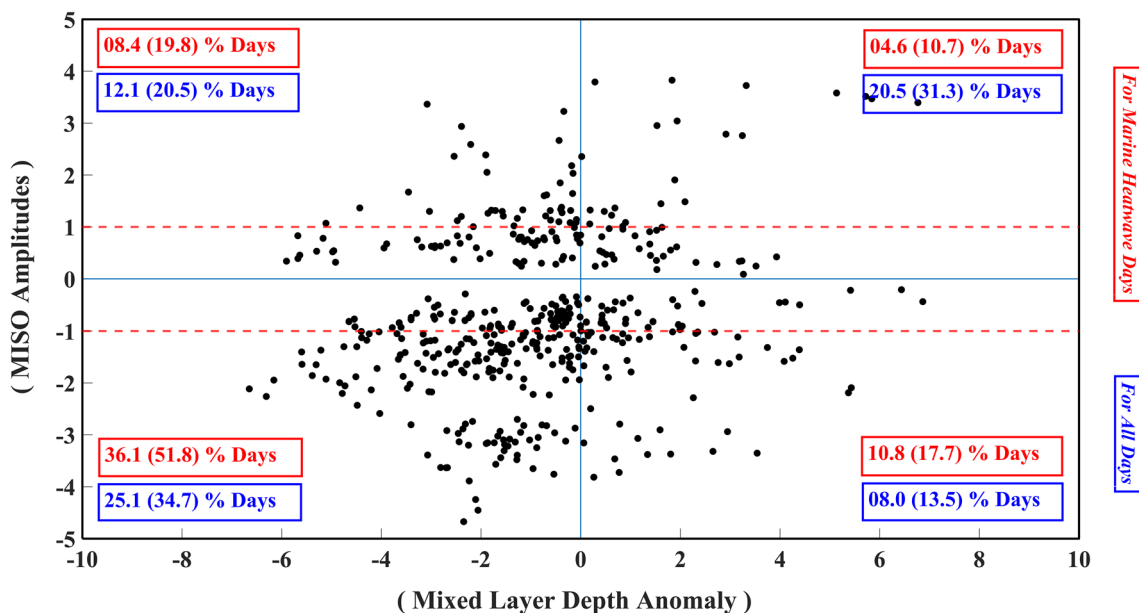

Fig. 11 Scatter plot of the number of MHW days from 1998 to 2020 irrespective of MISO amplitudes. Black-filled circles in the scattered diagram are representing the MHW days. The upper and lower horizontal red dotted lines in the diagram are representing the lines with MISO amplitudes equal to +1 (for MISO active phases) and −1 (for MISO break phases) respectively. The red and blue boxes inside the

diagram are showing the percentage of days associated with the conditions mentioned in the red and blue boxes respectively. Inside the red and blue boxes, the percentage within the bracket and just in front of the bracket represent the percentage considering MISO all amplitudes and MISO amplitudes > 1/ < −1 respectively

values (MISO amplitudes and MLD anomalies) are negative and a very less number of MHW days will be over the north BoB when both the values are positive during the boreal summer monsoon seasons (Fig. 11).

The results suggest that more than 51% (when all MISO amplitudes are considered irrespective of signs) and 36% (when MISO amplitudes are less than –1) of MHW days are associated with the case when both the MISO amplitudes as well as MLD anomalies are negative (Fig. 11). On the other hand, it is shown that 10.7%, 19.8%, and 17.7% MHW days are linked with conditions 1, 2, and 4 respectively for the case of all MISO amplitudes, whereas, for only MISO amplitude greater than 1, these percentages of MHW days are respectively 4.6% and 8.4% (conditions 1 and 2), and if MISO amplitudes are less than – 1, the percentage value is 10.8% (condition 4). This confirms that MISO active and break phases are also responsible for the modulation of SST and could trigger the MHW events over the north BoB during the boreal summer monsoon seasons. Similarly, for all boreal summer monsoon days including the MHW days, the percentage of summer monsoon days belonging to condition 3 is usually higher than the days associated with the other three conditions (Fig. 11). That implies that MISO break phases are mainly coupled with shallower MLD over the BoB. The exact relationship is complex to understand fully but it is clear that local ocean-atmospheric conditions are very important to recognize the characteristics of MHW events which are mainly driven by the air-sea heat flux over BoB during the boreal summer monsoon season.

The area average of sea surface salinity (SSS) anomaly is computed over the study region and the scattered distribution of the area average of SSS anomaly values (1993–2020) and the MISO amplitudes (1998–2020) associated with the MHW days (a total of 473 MHW days from 1998 to 2020) are shown in the Fig. S6. Further, the percentage of days associated with the four conditions—when both the MISO amplitudes and SSS anomaly values are positive; when MISO amplitudes > 0 but SSS anomaly values < 0; when both the MISO amplitudes and SSS anomaly values are negative; when MISO amplitudes < 0 but SSS anomaly values > 0 are computed respectively. The freshwater intrusion over the sea surface (negative SSS anomalies) and the break phases of MISO (negative MISO amplitudes) during the boreal summer monsoon season, both can generate a favourable background for the genesis and persistence of MHW events over the north BoB. The results suggest that more than 34% (when all MISO amplitudes are considered irrespective of signs) and 24% (when MISO amplitudes are less than –1) of MHW days are associated with the case when both the MISO amplitudes and SSS anomalies are negative. Similar to the variations of MLD anomalies with MISO amplitudes, where the present study found that more than 51% (when all MISO amplitudes are considered

irrespective of signs) and 36% (when MISO amplitudes are less than –1) of MHW days are associated with the case when both the MISO amplitudes as well as MLD anomalies are negative (Fig. 11).

Few studies have performed a heat budget analysis of the mixed layer to identify the primary drivers of these extreme MHW events (e.g., Amaya et al. 2021; Schlegel et al. 2021; Elzahaby et al. 2022; Mawren et al. 2022). For example, based on the heat budget analysis over the NIO, Saranya et al. (2022) showed that over the north BoB the SST variability during the boreal summer monsoon season is mostly attributed to net heat flux, the exact role of the advection term is minimal in the analysis. On the other hand, the role of the LHF and the net SWR terms was significant among the heat flux terms. So, with ocean dynamics, the role of air-sea heat flux is also very crucial in the occurrences and persistence of MHW events over the north BoB during the boreal summer monsoon season.

5 Conclusions

In this present study, an increasing trend in the area-average SST anomaly, the number and total duration of MHW events (yearly) over north BoB during the boreal summer monsoon season are found to be increasing in the recent decades. The composite time series of the SST anomalies for all MHW events' evolution showed the presence of three phases, which are the developing, mature, and decay phases. The north BoB has experienced a total of 38 MHW events associated with overall 624 MHW days during the boreal summer monsoon seasons from 1982 to 2021. However, the north BoB has experienced more than 2/3rd of the total MHW events in the recent two decades. RAMA buoy's observation at the grid point 90° E and 15° N also showed a total of 12 MHW events accompanied by 146 days for the period of the last 14 years (2008-2021) (Figure S2). Among 146 MHW days, a total of 141 days are common in both NOAA OISST and RAMA buoy data, suggesting the robustness of results obtained here. The composite analysis during MHW days suggests that positive anomalies of SWR, SSHA, NHF, and comparatively high air temperature than normal over the study region are responsible for the higher SST values over the north BoB. In addition to this, the negative anomalies of the wind speed, TCC, and wind stress over the study region reveal the importance of the oceanic-atmospheric coupling in driving MHW events during the boreal summer monsoon season events during the boreal summer monsoon season. The negative TCC anomaly is mainly responsible for enhanced SWR over the north BoB. On the other hand, the equatorial wave activity supports the convergence of warm upper water over the MHW events' region in the BoB as indicated by the positive sea surface height anomalies. In

terms of the consequences of MHW events, the present study has also reported the changes in the surface chlorophyll-*a* concentration (a proxy for primary productivity) over the BoB during the boreal summer monsoon season. Interestingly, it is found that there is a reduction in the concentration of Chl-*a* in the upper water column which is responsible for the negative anomalies of Chl-*a* concentration over north BoB during the MHW days (Fig. 12).

Most importantly, this study focused on understanding the impact of MISO on the occurrences of MHW events over the north BoB. Our analysis suggests that higher SST anomalies and more MHW days are associated with the break phases of MISO. This is mainly due to enhanced SWR associated with the very less cloud cover over the north BoB. On the other hand, a very less number of MHW days are present in the active phases of MISO. During the MHW days, a shallower extent of MLD is also evident over the north BoB, based on the mixed layer heat budget analysis, the present study can also conclude that the role of the heat-flux term in the temperature tendency equation (e.g., Saranya et al. 2022) is crucial over the advection term in driving the MHW events. Using a statistical analysis, the present study also showed that a high percentage of MHW days occurred over the north BoB during the MISO break phases, when there is a shallower extent of MLD than usual in the boreal summer monsoon season. Northward propagation of SST anomaly is also prominent during the evolution of MHW events over the study region. Further, Wyatt et al. (2023) showed that MHW events also have a very close relationship with the mesoscale eddies, however, Gulakaram et al. (2023) found an unusual response of SST associated with mesoscale eddies over the BoB, so, finding the exact relationship of the mesoscale eddies with the occurrence of MHW events
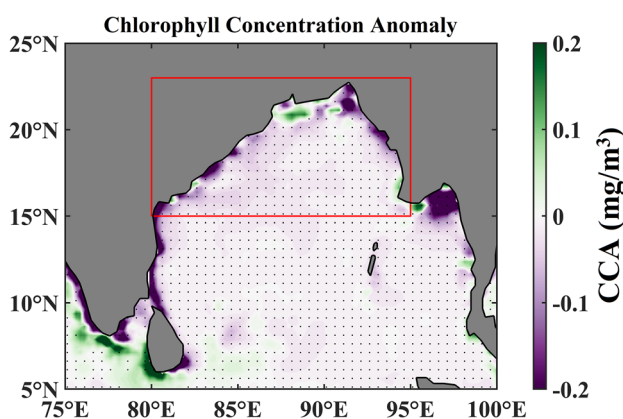
over the BoB is also worth taking in the recent warming scenarios. Furthermore, both observations and model simulations have shown that the intensity of the active phases of MISO has undergone a weakening over the last six decades (Karmakar et al. 2015, 2017), attributed to the occurrences of MHW events over the north BoB during the boreal summer monsoon season. So, the socioeconomic consequences of MHW events over the eastern coastal regions of India are also projected to be intense as well as widespread throughout the twenty-first century.

Declarations

Conflict of interest The authors declare that they have no known competing financial interests or personal relationships that could have appeared to influence the work reported in this paper.

Fig. 12 The composite anomaly of Chlorophyll-*a* concentration (CCA in mg/m^3) over the BoB during the MHW days in the boreal summer monsoon season from 1998 to 2020. The red rectangular box is representing the study area over the BoB. Anomaly values that are significant at a 95% confidence level are indicated by stippling (black dots)

References

Aboelkhair H, Mohamed B, Morsy M, Nagy H (2023) Co-occurrence of atmospheric and oceanic heatwaves in the Eastern Mediterranean over the last four decades. Remote Sensing 15(7):1841. https://doi.org/10.3390/rs15071841

Albert J, Gulakaram VS, Vissa NK, Bhaskaran PK, Dash MK (2023) Recent warming trends in the Arabian Sea: causative factors and physical mechanisms. Climate 11(2):35. https://doi.org/10.3390/cli11020035

Amaya DJ, Alexander MA, Capotondi A, Deser C, Karnauskas KB, Miller AJ, Mantua NJ (2021) Are long-term changes in mixed layer depth influencing North Pacific Marine heatwaves? Bull Am Meteorol Soc 102(1):S59–S66. https://doi.org/10.1175/BAMS-D-20-0144.1

Aoki LR, McGlathery KJ, Wiberg PL, Oreska MPJ, Berger AC, Berg P, Orth RJ (2021) Seagrass Recovery Following Marine Heat Wave Influences Sediment Carbon Stocks. Front Mar Sci 7:576784. https://doi.org/10.3389/fmars.2020.576784

Banzon V, Smith TM, Chin TM, Liu C, Hankins W (2016) A long-term record of blended satellite and in situ sea-surface temperature for climate monitoring, modeling and environmental studies. Earth Syst Sci Data 8:165–176. https://doi.org/10.5194/essd-8-165-2016

Behr L, Petalas S, Jaeger M, Xoplaki E, Tragou E, Gogou A, Zervakis V (2021) Atmosphere-Ocean compound heat wave events in the Eastern Mediterranean. https://doi.org/10.5194/egusphere-egu21-9583

Benthuysen JA, Oliver ECJ, Feng M, Marshall AG (2018) Extreme marine warming across tropical Australia during Austral summer 2015–2016. J Geophys Res Oceans 123(2):1301–1326. https://doi.org/10.1002/2017JC013326

Brauko KM, Cabral A, Costa NV, Hayden J, Dias CEP, Leite ES, Westphal RD, Mueller CM, Hall-Spencer JM, Rodrigues RR, Rörig LR, Pagliosa PR, Fonseca AL, Alarcon OE, Horta PA (2020) Marine heatwaves, sewage and eutrophication combine to trigger deoxygenation and biodiversity loss: a SW Atlantic Case Study. Front Mar Sci 7:590258. https://doi.org/10.3389/fmars.2020.590258

Cai Y, Chen Z, Du Y (2022) The role of Indian Ocean warming on extreme rainfall in central China during early summer 2020: without significant El Niño influence. Clim Dyn 59(3–4):951–960. https://doi.org/10.1007/s00382-022-06165-9

Cao D, Xu K, Huang Q-L, Tam C-Y, Chen S, He Z, Wang W (2022) Exceptionally prolonged extreme heat waves over South China in early summer 2020: The role of warming in the tropical Indian Ocean. Atmos Res 278:106335. https://doi.org/10.1016/j.atmosres.2022.106335

Carvalho KS, Smith TE, Wang S (2021) Bering Sea marine heatwaves: Patterns, trends and connections with the Arctic. J Hydrol 600:126462. https://doi.org/10.1016/j.jhydrol.2021.126462

Chatterjee A, Anil G, Shenoy LR (2022) Marine heatwaves in the Arabian Sea. Ocean Sci 18(3):639–657. https://doi.org/10.5194/os-18-639-2022

Chen K, Gawarkiewicz GG, Lentz SJ, Bane JM (2014) Diagnosing the warming of the Northeastern U.S. Coastal Ocean in 2012: a linkage between the atmospheric jet stream variability and ocean response. J Geophys Res Oceans 119(1):218–227. https://doi.org/10.1002/2013JC009393

Cheung WWL, Frölicher TL (2020) Marine heatwaves exacerbate climate change impacts for fisheries in the northeast Pacific. Sci Rep 10(1):6678. https://doi.org/10.1038/s41598-020-63650-z

Chiswell SM, Sutton PJH (2020) Relationships between long-term ocean warming, marine heat waves and primary production in the New Zealand region. NZ J Mar Freshw Res 54(4):614–635. https://doi.org/10.1080/00288330.2020.1713181

Cook F, Smith RO, Roughan M, Cullen NJ, Shears N, Bowen M (2022) Marine heatwaves in shallow coastal ecosystems are coupled with the atmosphere: insights from half a century of daily in situ temperature records. Front Clim 4:1012022. https://doi.org/10.3389/fclim.2022.1012022

Dayan H, McAdam R, Juza M, Masina S, Speich S (2023) Marine heat waves in the Mediterranean Sea: an assessment from the surface to the subsurface to meet national needs. Front Mar Sci 10:1045138. https://doi.org/10.3389/fmars.2023.1045138

Deshpande NR, Goswami BN (2014) Modulation of the diurnal cycle of rainfall over India by intraseasonal variations of Indian summer monsoon. Int J Climatol 34(3):793–807. https://doi.org/10.1002/joc.3719

Dey A, Chattopadhyay R, Joseph S, Kaur M, Mandal R, Phani R, Sahai AK, Pattanaik DR (2022) The intraseasonal fluctuation of Indian summer monsoon rainfall and its relation with monsoon intraseasonal oscillation (MISO) and Madden Julian oscillation (MJO). Theoret Appl Climatol 148(1–2):819–831. https://doi.org/10.1007/s00704-022-03970-4

Di Lorenzo E, Mantua N (2016) Multi-year persistence of the 2014/15 North Pacific marine heatwave. Nat Clim Change 6(11):1042–1047. https://doi.org/10.1038/nclimate3082

Dodrill TN, Pan Y, Peterson TD (2023) River discharge mediates extent of phytoplankton and harmful algal bloom habitat in the Columbia River Estuary (USA) during North Pacific Marine Heat Waves. Estuaries Coasts 46(1):166–181. https://doi.org/10.1007/s12237-022-01129-y

Du Y, Xie S-P, Huang G, Hu K (2009) Role of air-sea interaction in the long persistence of El Niño-induced North Indian Ocean warming. J Clim 22(8):2023–2038. https://doi.org/10.1175/2008JCLI2590.1

Durand F, Shankar D, Birol F, Shenoi SSC (2009) Spatiotemporal structure of the East India Coastal Current from satellite altimetry. J Geophys Res 114(C2):C02013. https://doi.org/10.1029/2008JC004807

Elzahaby Y, Schaeffer A, Roughan M, Delaux S (2021) Oceanic circulation drives the deepest and longest marine heatwaves in the East Australian current system. Geophys Res Lett. https://doi.org/10.1029/2021GL094785

Elzahaby Y, Schaeffer A, Roughan M, Delaux S (2022) Why the mixed layer depth matters when diagnosing marine heatwave drivers using a heat budget approach. Front Clim 4:838017. https://doi.org/10.3389/fclim.2022.838017

Feng M, McPhaden MJ, Xie S-P, Hafner J (2013) La Niña forces unprecedented Leeuwin Current warming in 2011. Sci Rep 3(1):1277. https://doi.org/10.1038/srep01277

Gao X, Li G, Liu J, Long S-M (2022) The trend and interannual variability of marine heatwaves over the Bay of Bengal. Atmosphere 13(3):469. https://doi.org/10.3390/atmos13030469

George JV, Vinayachandran PN, Vijith V, Thushara V, Nayak AA, Pargaonkar SM, Amol P, Vijaykumar K, Matthews AJ (2019) Mechanisms of barrier layer formation and erosion from in situ observations in the Bay of Bengal. J Phys Oceanogr 49(5):1183–1200. https://doi.org/10.1175/JPO-D-18-0204.1

Goswami BB, Murtugudde R, An S-I (2022) Role of the Bay of Bengal warming in the Indian summer monsoon rainfall trend. Clim Dyn 59(5–6):1733–1751. https://doi.org/10.1007/s00382-021-06068-1

Gulakaram VS, Vissa NK, Bhaskaran PK (2018) Role of mesoscale eddies on atmospheric convection during summer monsoon season over the Bay of Bengal: a case study. J Ocean Eng Sci 3(4):343–354. https://doi.org/10.1016/j.joes.2018.11.002

Gulakaram VS, Vissa NK, Bhaskaran PK (2023) Mesoscale eddies with anomalous sea surface temperature and its relation with atmospheric convection over the North Indian Ocean. Int J Climatol. https://doi.org/10.1002/joc.8018

Habibullah AD, Tarya A, Ningsih NS, Putri MR (2023) Marine heatwaves in the Indonesian fisheries management areas. J Mar Sci Eng 11(1):161. https://doi.org/10.3390/jmse11010161

Hamdeno M, Nagy H, Ibrahim O, Mohamed B (2022) Responses of satellite chlorophyll-a to the extreme sea surface temperatures over the Arabian and Omani Gulf. Remote Sensing 14(18):4653. https://doi.org/10.3390/rs14184653

Han W, Zhang L, Meehl G, Kido S, Tozuka T, Li Y, McPhaden M, Hu A, Cazenave A, Rosenbloom N, Strand G, West B (2021).

Climate-driven sea level extremes compounded by marine heatwaves in coastal Indonesia. https://doi.org/10.21203/rs.3.rs-310860/v1

Hersbach H, Bell B, Berrisford P, Hirahara S, Horányi A, Muñoz-Sabater J, Nicolas J, Peubey C, Radu R, Schepers D, Simmons A, Soci C, Abdalla S, Abellan X, Balsamo G, Bechtold P, Biavati G, Bidlot J, Bonavita M, Thépaut J (2020) The ERA5 global reanalysis. Q J R Meteorol Soc 146(730):1999–2049. https://doi.org/10.1002/qj.3803

Hobday AJ, Alexander LV, Perkins SE, Smale DA, Straub SC, Oliver ECJ, Benthuysen JA, Burrows MT, Donat MG, Feng M, Holbrook NJ, Moore PJ, Scannell HA, Sen Gupta A, Wernberg T (2016) A hierarchical approach to defining marine heatwaves. Prog Oceanogr 141:227–238. https://doi.org/10.1016/j.pocean.2015.12.014

Holbrook NJ, Scannell HA, Sen Gupta A, Benthuysen JA, Feng M, Oliver ECJ, Alexander LV, Burrows MT, Donat MG, Hobday AJ, Moore PJ, Perkins-Kirkpatrick SE, Smale DA, Straub SC, Wernberg T (2019) A global assessment of marine heatwaves and their drivers. Nat Commun 10(1):2624. https://doi.org/10.1038/s41467-019-10206-z

Hsu P-C, Lee J-Y, Ha K-J, Tsou C-H (2017) Influences of boreal summer intraseasonal oscillation on heat waves in monsoon Asia. J Clim 30(18):7191–7211. https://doi.org/10.1175/JCLI-D-16-0505.1

Hu S, Zhang L, Qian S (2020) Marine heatwaves in the Arctic Region: variation in different ice covers. Geophys Res Lett. https://doi.org/10.1029/2020GL089329

Huang B, Liu C, Banzon V, Freeman E, Graham G, Hankins B, Smith T, Zhang H-M (2021a) Improvements of the daily optimum interpolation sea surface temperature (DOISST) version 2.1. J Clim 34(8):2923–2939. https://doi.org/10.1175/JCLI-D-20-0166.1

Huang B, Wang Z, Yin X, Arguez A, Graham G, Liu C, Smith T, Zhang H (2021b) Prolonged marine heatwaves in the Arctic: 1982–2020. Geophys Res Lett. https://doi.org/10.1029/2021GL095590

Intergovernmental Panel on Climate Change (IPCC) (2023) Ocean, cryosphere and sea level change. In Climate Change 2021 – The physical science basis: working group I contribution to the sixth assessment report of the Intergovernmental Panel on Climate Change (pp 1211–1362). Cambridge: Cambridge University Press. https://doi.org/10.1017/9781009157896.011

Jana S, Gangopadhyay A, Chakraborty A (2015) Impact of seasonal river input on the Bay of Bengal simulation. Cont Shelf Res 104:45–62. https://doi.org/10.1016/j.csr.2015.05.001

Jones T, Parrish JK, Peterson WT, Bjorkstedt EP, Bond NA, Ballance LT, Bowes V, Hipfner JM, Burgess HK, Dolliver JE, Lindquist K, Lindsey J, Nevins HM, Robertson RR, Roletto J, Wilson L, Joyce T, Harvey J (2018) Massive mortality of a Planktivorous seabird in response to a marine heatwave. Geophys Res Lett 45(7):3193–3202. https://doi.org/10.1002/2017GL076164

Karmakar N, Chakraborty A, Nanjundiah RS (2015) Decreasing intensity of monsoon low-frequency intraseasonal variability over India. Environ Res Lett 10(5):054018. https://doi.org/10.1088/1748-9326/10/5/054018

Karmakar N, Chakraborty A, Nanjundiah RS (2017) Increased sporadic extremes decrease the intraseasonal variability in the Indian summer monsoon rainfall. Sci Rep 7(1):7824. https://doi.org/10.1038/s41598-017-07529-6

Konda G, Vissa NK (2019) Intraseasonal convection and air-sea fluxes over the indian monsoon region revealed from the Bimodal ISO index. Pure Appl Geophys 176(8):3665–3680. https://doi.org/10.1007/s00024-019-02119-1

Konda G, Vissa NK (2021) Assessment of ocean-atmosphere interactions for the boreal summer intraseasonal oscillations in CMIP5

models over the Indian Monsoon Region. Asia-Pac J Atmos Sci 57(4):717–739. https://doi.org/10.1007/s13143-021-00228-3

Krishnamohan KS, Vialard J, Lengaigne M, Masson S, Samson G, Pous S, Neetu S, Durand F, Shenoi SSC, Madec G (2019) Is there an effect of Bay of Bengal salinity on the northern Indian Ocean climatological rainfall? Top Stud Oceanogr 166:19–33. https://doi.org/10.1016/j.dsr2.2019.04.003

Krishnan P, Roy SD, George G, Srivastava RC, Anand A, Murugesan S, Kaliyamoorthy M, Vikas N, Soundararajan R (2011) Elevated sea surface temperature during May 2010 induces mass bleaching of corals in the Andaman. Curr Sci 100(1):111–117

Lam VWY, Chavanich S, Djoundourian S, Dupont S, Gaill F, Holzer G, Isensee K, Katua S, Mars F, Metian M, Hall-Spencer JM (2019) Dealing with the effects of ocean acidification on coral reefs in the Indian Ocean and Asia. Reg Stud Mar Sci 28:100560. https://doi.org/10.1016/j.rsma.2019.100560

Le Grix N, Zscheischler J, Laufkötter C, Rousseaux CS, Frölicher TL (2021) Compound high-temperature and low-chlorophyll extremes in the ocean over the satellite period. Biogeosciences 18(6):2119–2137. https://doi.org/10.5194/bg-18-2119-2021

Li B, Zhou L, Qin J, Murtugudde R (2022) Increase in intraseasonal rainfall driven by the Arabian Sea warming in recent decades. Geophys Res Lett. https://doi.org/10.1029/2022GL100536

Lin X, Qiu Y, Wang J, Teng H, Ni X, Liang K (2023) Seasonal diversity of El Niño-induced marine heatwave increases in the Bay of Bengal. Geophys Res Lett. https://doi.org/10.1029/2022GL100807

Manta G, Mello S, Trinchin R, Badagian J, Barreiro M (2018) The 2017 record marine heatwave in the Southwestern Atlantic Shelf. Geophys Res Lett 45(22):12449–12456. https://doi.org/10.1029/2018GL081070

Masud-Ul-Alam Md, Khan MdAI, Barrett BS, Rivero-Calle S (2022) Surface temperature and salinity in the northern Bay of Bengal: In situ measurements compared with satellite observations and model output. J Appl Remote Sens. https://doi.org/10.1117/1.JRS.16.018502

Mawren D, Hermes J, Reason CJC (2022) Marine heatwaves in the Mozambique Channel. Clim Dyn 58(1–2):305–327. https://doi.org/10.1007/s00382-021-05909-3

McPhaden MJ, Meyers G, Ando K, Masumoto Y, Murty VSN, Ravichandran M, Syamsudin F, Vialard J, Yu L, Yu W (2009) RAMA: the research moored array for African–Asian–Australian monsoon analysis and prediction. Bull Am Meteor Soc 90(4):459–480. https://doi.org/10.1175/2008BAMS2608.1

Mills K, Pershing A, Brown C, Chen Y, Chiang F-S, Holland D, Lehuta S, Nye J, Sun J, Thomas A, Wahle R (2013) Fisheries management in a changing climate: lessons from the 2012 ocean heat wave in the Northwest Atlantic. Oceanography. https://doi.org/10.5670/oceanog.2013.27

Mohamed B, Nilsen F, Skogseth R (2022) Marine Heatwaves Characteristics in the Barents Sea Based on High Resolution Satellite Data (1982–2020). Front Mar Sci 9:821646. https://doi.org/10.3389/fmars.2022.821646

Mohapatra M, Nayak DP, Sharma RP, Bandyopadhyay BK (2013) Evaluation of official tropical cyclone track forecast over north Indian Ocean issued by India Meteorological Department. J Earth Syst Sci 122(3):589–601. https://doi.org/10.1007/s12040-013-0291-1

Noh KM, Lim H-G, Kug J-S (2022) Global chlorophyll responses to marine heatwaves in satellite ocean color. Environ Res Lett 17(6):064034. https://doi.org/10.1088/1748-9326/ac70ec

Oliver ECJ (2019) Mean warming not variability drives marine heatwave trends. Clim Dyn 53(3–4):1653–1659. https://doi.org/10.1007/s00382-019-04707-2

Oliver ECJ, Benthuysen JA, Bindoff NL, Hobday AJ, Holbrook NJ, Mundy CN, Perkins-Kirkpatrick SE (2017) The unprecedented

2015/16 Tasman Sea marine heatwave. Nat Commun 8(1):16101. https://doi.org/10.1038/ncomms16101

Oliver ECJ, Donat MG, Burrows MT, Moore PJ, Smale DA, Alexander LV, Benthuysen JA, Feng M, Sen Gupta A, Hobday AJ, Holbrook NJ, Perkins-Kirkpatrick SE, Scannell HA, Straub SC, Wernberg T (2018) Longer and more frequent marine heatwaves over the past century. Nat Commun 9(1):1324. https://doi.org/10.1038/s41467-018-03732-9

Pai DS, Sridhar L, Ramesh Kumar MR (2016) Active and break events of Indian summer monsoon during 1901–2014. Clim Dyn 46(11–12):3921–3939. https://doi.org/10.1007/s00382-015-2813-9

Pascual A, Faugère Y, Larnicol G, Le Traon P-Y (2006) Improved description of the ocean mesoscale variability by combining four satellite altimeters. Geophys Res Lett 33(2):L02611. https://doi.org/10.1029/2005GL024633

Pathmeswaran C, Sen Gupta A, Perkins-Kirkpatrick SE, Hart MA (2022) Exploring potential links between co-occurring coastal terrestrial and marine heatwaves in Australia. Front Clim 4:792730. https://doi.org/10.3389/fclim.2022.792730

Patterson Edward JK, Mathews G, Diraviya Raj K, Laju RL, Selva Bharath M, Arasamuthu A, Dinesh Kumar P, Bilgi DS, Malleshappa H (2018) Coral mortality in the Gulf of Mannar, Southeastern India, due to bleaching caused by elevated sea temperature in 2016. Curr Sci 114(09):1967. https://doi.org/10.18520/cs/v114/i09/1967-1972

Pearce A (2011) The "marine heat wave" off Western Australia during the summer of 2010/11. Western Australian Fisheries and Marine Research Laboratories

Pearce AF, Feng M (2013) The rise and fall of the "marine heat wave" off Western Australia during the summer of 2010/2011. J Mar Syst 111–112:139–156. https://doi.org/10.1016/j.jmarsys.2012.10.009

Pietri A, Colas F, Mogollon R, Espinoza-Morriberón D, Chamorro A, Tam J, Gutiérrez D (2020) Characterization and evolution of marine heat waves in the peruvian upwelling system. 10.5194/egusphere-egu2020-20036

Prasanna Kumar S, Muraleedharan PM, Prasad TG, Gauns M, Ramaiah N, de Souza SN, Sardesai S, Madhupratap M (2002) Why is the Bay of Bengal less productive during summer monsoon compared to the Arabian Sea? Geophys Rese Lett 29(24):88-1–88-4. https://doi.org/10.1029/2002GL016013

Praveen Kumar B, Vialard J, Lengaigne M, Murty VSN, McPhaden MJ (2012) TropFlux: Air-sea fluxes for the global tropical oceans-description and evaluation. Clim Dyn 38(7–8):1521–1543. https://doi.org/10.1007/s00382-011-1115-0

Praveen Kumar B, Vialard J, Lengaigne M, Murty VSN, McPhaden MJ, Cronin MF, Pinsard F, Gopala Reddy K (2013) TropFlux wind stresses over the tropical oceans: Evaluation and comparison with other products. Clim Dyn 40(7–8):2049–2071. https://doi.org/10.1007/s00382-012-1455-4

Qi R, Zhang Y, Du Y, Feng M (2022) Characteristics and Drivers of Marine Heatwaves in the Western Equatorial Indian Ocean. J Geophys Res Oceans. https://doi.org/10.1029/2022JC018732

Rajeevan M, Gadgil S, Bhate J (2010) Active and break spells of the Indian summer monsoon. J Earth Syst Sci 119(3):229–247. https://doi.org/10.1007/s12040-010-0019-4

Rao RR, Girish Kumar MS, Ravichandran M, Rao AR, Gopalakrishna VV, Thadathil P (2010) Interannual variability of Kelvin wave propagation in the wave guides of the equatorial Indian Ocean, the coastal Bay of Bengal, and the southeastern Arabian Sea during 1993–2006. Oceanogr Res Papers 57(1):1–13. https://doi.org/10.1016/j.dsr.2009.10.008

Rathore S, Goyal R, Jangir B, Ummenhofer CC, Feng M, Mishra M (2022) Interactions between a marine heatwave and tropical cyclone amphan in the Bay of Bengal in 2020. Front Clim 4:861477. https://doi.org/10.3389/fclim.2022.861477

Reynolds RW, Smith TM, Liu C, Chelton DB, Casey KS, Schlax MG (2007) Daily high-resolution-blended analyses for sea surface temperature. J Clim 20(22):5473–5496. https://doi.org/10.1175/2007JCLI1824.1

Roxy M (2014) Sensitivity of precipitation to sea surface temperature over the tropical summer monsoon region-And its quantification. Clim Dyn 43(5–6):1159–1169. https://doi.org/10.1007/s00382-013-1881-y

Roxy M, Tanimoto Y (2007) Role of SST over the Indian Ocean in Influencing the Intraseasonal Variability of the Indian Summer Monsoon. J Meteorol Soc Jpn Ser II 85(3):349–358. https://doi.org/10.2151/jmsj.85.349

Roxy MK, Modi A, Murtugudde R, Valsala V, Panickal S, Prasanna Kumar S, Ravichandran M, Vichi M, Lévy M (2016) A reduction in marine primary productivity driven by rapid warming over the tropical Indian Ocean. Geophys Res Lett 43(2):826–833. https://doi.org/10.1002/2015GL066979

Sadhuram Y, Rao BP, Rao DP, Shastri PNM, Subrahmanyam MV (2004) Seasonal variability of cyclone heat potential in the Bay of Bengal. Nat Hazards 32(2):191–209. https://doi.org/10.1023/B:NHAZ.0000031313.43492.a8

Salinger MJ, Renwick J, Behrens E, Mullan AB, Diamond HJ, Sirguey P, Smith RO, Trought MCT, Alexander L, Cullen NJ, Fitzharris BB, Hepburn CD, Parker AK, Sutton PJ (2019) The unprecedented coupled ocean-atmosphere summer heatwave in the New Zealand region 2017/18: Drivers, mechanisms, and impacts. Environ Res Lett 14(4):044023. https://doi.org/10.1088/1748-9326/ab012

Saranya JS, Roxy MK, Dasgupta P, Anand A (2022) Genesis and trends in marine heatwaves over the tropical Indian Ocean and their interaction with the Indian Summer monsoon. J Geophys Res Oceans. https://doi.org/10.1029/2021JC017427

Scannell HA, Pershing AJ, Alexander MA, Thomas AC, Mills KE (2016) Frequency of marine heatwaves in the North Atlantic and North Pacific since 1950. Geophys Res Lett 43(5):2069–2076. https://doi.org/10.1002/2015GL067308

Schaeffer A, Roughan M (2017) Subsurface intensification of marine heatwaves off southeastern Australia: the role of stratification and local winds. Geophys Res Lett 44(10):5025–5033. https://doi.org/10.1002/2017GL073714

Schlegel RW, Oliver ECJ, Chen K (2021) Drivers of marine heatwaves in the Northwest Atlantic: the role of air-sea interaction during onset and decline. Front Mar Sci 8:627970. https://doi.org/10.3389/fmars.2021.627970

Schott FA, Xie S-P, McCreary JP (2009) Indian Ocean circulation and climate variability. Rev Geophys 47(1):RG1002. https://doi.org/10.1029/2007RG000245

Sen Gupta A, Thomsen M, Benthuysen JA, Hobday AJ, Oliver E, Alexander LV, Burrows MT, Donat MG, Feng M, Holbrook NJ, Perkins-Kirkpatrick S, Moore PJ, Rodrigues RR, Scannell HA, Taschetto AS, Ummenhofer CC, Wernberg T, Smale DA (2020) Drivers and impacts of the most extreme marine heatwave events. Sci Rep 10(1):19359. https://doi.org/10.1038/s41598-020-75445-3

Seo H, Xie S-P, Murtugudde R, Jochum M, Miller AJ (2009) Seasonal effects of Indian Ocean freshwater forcing in a regional coupled model. J Clim 22(24):6577–6596. https://doi.org/10.1175/2009JCLI2990.1

Singh C, Dasgupta P (2017) Unraveling the spatio-temporal structure of the atmospheric and oceanic intra-seasonal oscillations during the contrasting monsoon seasons. Atmos Res 192:48–57. https://doi.org/10.1016/j.atmosres.2017.03.020

Sridevi B, Sarma VVSS (2021) Role of river discharge and warming on ocean acidification and pCO_2 levels in the Bay of Bengal. Tellus B Chem Phys Meteorol 73(1):1971924. https://doi.org/10.1080/16000889.2021.1971924

Suhas E, Neena JM, Goswami BN (2013) An Indian monsoon intra-seasonal oscillations (MISO) index for real time monitoring and forecast verification. Clim Dyn 40(11–12):2605–2616. https://doi.org/10.1007/s00382-012-1462-5

Takagi S, Kuroda H, Hasegawa N, Watanabe T, Unuma T, Taniuchi Y, Yokota T, Izumida D, Nakagawa T, Kurokawa T, Azumaya T (2022) Controlling factors of large-scale harmful algal blooms with Karenia selliformis after record-breaking marine heatwaves. Front Mar Sci 9:939393. https://doi.org/10.3389/fmars.2022.939393

Vecchi GA, Harrison DE (2002) Monsoon breaks and subseasonal sea surface temperature variability in the Bay of Bengal. J Clim 15(12):1485–1493. https://doi.org/10.1175/1520-0442(2002)015%3c1485:MBASSS%3e2.0.CO;2

Vinayachandran PN (2005) Bifurcation of the East India Coastal Current east of Sri Lanka. Geophys Res Lett 32(15):L15606. https://doi.org/10.1029/2005GL022864

Vinayachandran PN, Murty VSN, Ramesh Babu V (2002) Observations of barrier layer formation in the Bay of Bengal during summer monsoon. J Geophysi Res Oceans 107(C12):SRF 19-1-SRF 19-9. https://doi.org/10.1029/2001JC000831

Vinayachandran PNM, Masumoto Y, Roberts MJ, Huggett JA, Halo I, Chatterjee A, Amol P, Gupta GVM, Singh A, Mukherjee A, Prakash S, Beckley LE, Raes EJ, Hood R (2021) Reviews and syntheses: physical and biogeochemical processes associated with upwelling in the Indian Ocean. Biogeosciences 18(22):5967–6029. https://doi.org/10.5194/bg-18-5967-2021

Vissa NK, Satyanarayana ANV, Prasad Kumar B (2013) Comparison of mixed layer depth and barrier layer thickness for the Indian Ocean using two different climatologies. Int J Climatol 33(13):2855–2870. https://doi.org/10.1002/joc.3635

Vissa NK, Anandh PC, Gulakaram VS, Konda G (2021) Role and response of ocean–atmosphere interactions during Amphan (2020) super cyclone. Acta Geophys 69(5):1997–2010. https://doi.org/10.1007/s11600-021-00671-w

Wang Q, Zhang B, Zeng L, He Y, Wu Z, Chen J (2022) Properties and drivers of marine heat waves in the northern South China Sea. J Phys Oceanogr 52(5):917–927. https://doi.org/10.1175/JPO-D-21-0236.1

Wang S, Jing Z, Wu L, Sun S, Peng Q, Wang H, Zhang Y, Shi J (2023) Southern hemisphere eastern boundary upwelling systems emerging as future marine heatwave hotspots under greenhouse warming. Nat Commun 14(1):28. https://doi.org/10.1038/s41467-022-35666-8

Wheeler MC, Hendon HH (2004) An All-season real-time multivariate MJO index: development of an index for monitoring and prediction. Mon Weather Rev 132(8):1917–1932. https://doi.org/10.1175/1520-0493(2004)132%3c1917:AARMMI%3e2.0.CO;2

Wyatt ASJ, Leichter JJ, Washburn L, Kui L, Edmunds PJ, Burgess SC (2023) Hidden heatwaves and severe coral bleaching linked to mesoscale eddies and thermocline dynamics. Nat Commun 14(1):25. https://doi.org/10.1038/s41467-022-35550-5

Xie S-P, Annamalai H, Schott FA, McCreary JP (2002) Structure and mechanisms of South Indian Ocean climate variability. J Clim 15(8):864–878. https://doi.org/10.1175/1520-0442(2002)015%3c0864:SAMOSI%3e2.0.CO;2

Xu T, Newman M, Capotondi A, Stevenson S, Di Lorenzo E, Alexander MA (2022) An increase in marine heatwaves without significant changes in surface ocean temperature variability. Nat Commun 13(1):7396. https://doi.org/10.1038/s41467-022-34934-x

Zhang Y, Du Y (2021) Extreme IOD induced tropical Indian Ocean warming in 2020. Geosci Lett 8(1):37. https://doi.org/10.1186/s40562-021-00207-6

Zhang N, Feng M, Hendon HH, Hobday AJ, Zinke J (2017) Opposite polarities of ENSO drive distinct patterns of coral bleaching potentials in the southeast Indian Ocean. Sci Rep 7(1):2443. https://doi.org/10.1038/s41598-017-02688-y

Zhou Z-Q, Xie S-P, Zhang R (2021) Historic Yangtze flooding of 2020 tied to extreme Indian Ocean conditions. Proc Natl Acad Sci 118(12):e2022255118. https://doi.org/10.1073/pnas.2022255118

Zinke J, Hoell A, Lough JM, Feng M, Kuret AJ, Clarke H, Ricca V, Rankenburg K, McCulloch MT (2015) Coral record of southeast Indian Ocean marine heatwaves with intensified Western Pacific temperature gradient. Nat Commun 6(1):8562. https://doi.org/10.1038/ncomms9562